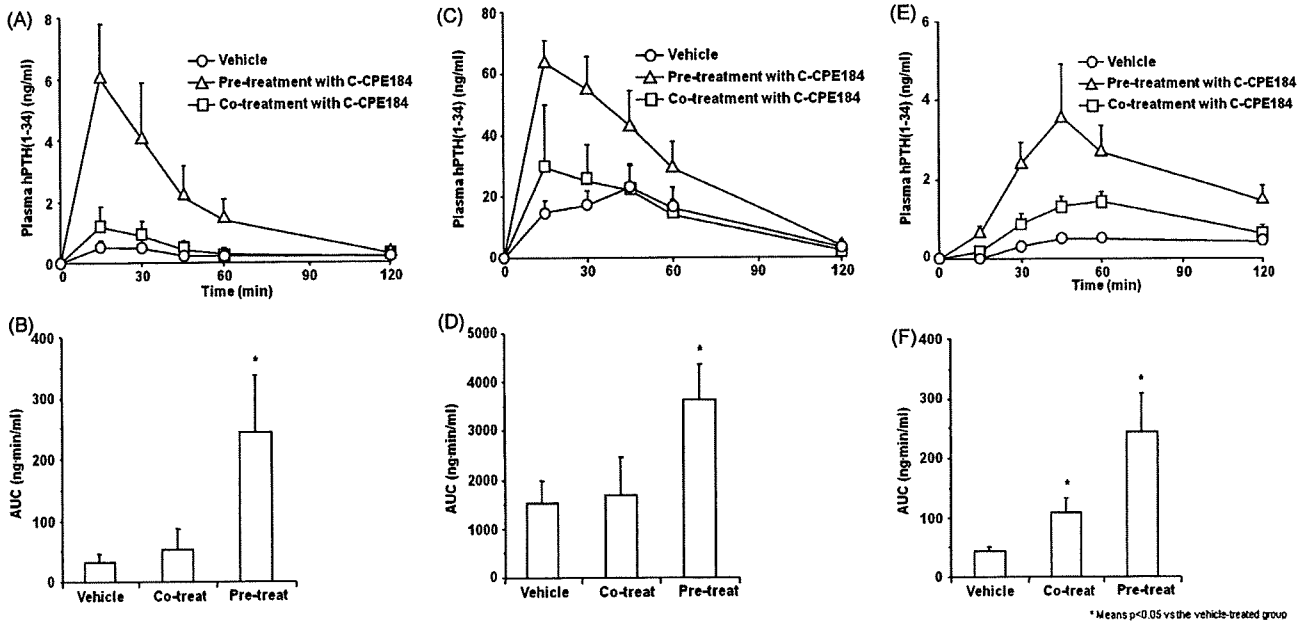

Fig. 1. Effect of C-CPE184 on mucosal absorption of hPTH(1-34) in rats. (A, B) Jejunal absorption of hPTH(1-34). Jejunum was co-treated with hPTH(1-34) (100 μg) and C-CPE184 (20 μg), or jejunum was treated with hPTH(1-34) 4 h after treatment with C-CPE184. (C, D) Pulmonary absorption of hPTH(1-34). hPTH(1-34) (150 μg) was pulmonary administered with C-CPE184 (5 μg) or 4 h after administration of C-CPE184. (E, F) Nasal absorption of hPTH(1-34). hPTH(1-34) (200 μg) was nasally administered with C-CPE184 (2 μg) or 4 h after administration of C-CPE184. Plasma hPTH(1-34) levels were measured at the indicated periods. Time-course changes in plasma hPTH(1-34) levels (A, C, E) and AUC from 0 to 120 min (B, D, F) were calculated. Data are mean ± SE (n = 3-6). Co-treat indicates co-treatment with both hPTH and C-CPE184, and Pre-treat indicates treatment with hPTH 4 h after C-CPE184-treatment. *Significantly different from the vehicle-treated group ($p < 0.05$).

Table 1
Parameters of mucosal absorption of hPTH(1-34) in C-CPE184-treated rats.

Treatments	Jejunum		Nasal		Pulmonary	
	Cmax (ng/ml)	BA (%)[a]	Cmax (ng ml)	BA (%)	Cmax (ng ml)	BA (%)
Vehicle	0.9 ± 0.3	0.4 ± 0.2	0.7 ± 0.1	0.3 ± 0.0	27.8 ± 6.5	14.6 ± 4.4
Co-treat	1.2 ± 0.6	0.6 ± 0.4	1.5 ± 0.2*	0.8 ± 0.2*	35.2 ± 18.9	14.9 ± 6.5
Pre-treat	6.0 ± 1.8*	2.7 ± 0.9*	3.6 ± 1.3	1.4 ± 0.4*	67.6 ± 7.5**	34.5 ± 6.6*

[a] BA (%) = (AUC/Dose)/(AUC iv/Dose iv).
Data are means ± SE.
*$p < 0.05$, **$p < 0.01$, as compared to vehicle-treated group.

increased 7.5-, 5.6- and 2.4-fold compared to the vehicle-treated group (Fig. 1 and Table 1).

3.2. Preparation of N-terminal-truncated C-CPE184-319 derivatives

The solubility of C-CPE184 is less than 0.3 mg/ml in PBS due to its hydrophobicity (Table 2). An increase in solubility without loss of claudin-4-modulating activity might improve the mucosal-absorption-enhancing activity of C-CPE184. Van Itallie et al. showed that the removal of the 10 N-terminal amino acids from C-CPE184 to yield C-CPE194 results in high solubility (10 mg/ml)

Table 2
Solubility of C-CPE184 and the N-terminal-truncated mutants.

Derivatives	Molecular size (kDa)	Solubility[a] (mg/ml)
C-CPE184	18.2	<0.3
C-CPE194	17.3	>10
C-CPE205	16.1	>4
C-CPE212	15.4	Insol.[b]
C-CPE219	14.7	Insol.
C-CPE224	14.2	Insol.

[a] Solvent is PBS.
[b] Insol., insoluble.

[26]. Although C-CPE194 is a claudin-4 binder, whether C-CPE194 modulates the TJ-barrier remains unclear. C-CPE194 contains nine β-sheets and one α-helix, and its 16 C-terminal amino acids are believed to comprise the claudin-4-binding region (Fig. 2A) [26,29]. Based on this information, we prepared five different N-terminal-truncated C-CPE184 derivatives: C-CPE194, which lacks the 10 N-terminal amino acids; C-CPE205, which is truncated prior to the β1-sheet; C-CPE212, which is truncated after the β1-sheet; C-CPE219, which is truncated after the α-helix; and C-CPE224, which is truncated before the β2-sheet (Fig. 2A). The C-CPEs were expressed in *E. coli* (Fig. 2B). The solubility of C-CPE194 (>10 mg/ml) and C-CPE205 (>4 mg/ml) in PBS was greater than that of C-CPE184 (<0.3 mg/ml) (Table 2). However, C-CPE212, C-CPE219 and C-CPE224 formed solid inclusion bodies in *E. coli*, and these inclusion bodies could not be dissolved without 2 M urea. Therefore, further experiments were performed with C-CPE184, C-CPE194 and C-CPE205.

3.3. Characterization of C-CPE194 and C-CPE205

To study the interaction between the C-CPEs and claudin-4, we performed ELISA with claudin-4-displaying BV, as described previously [24]. When C-CPEs were added to claudin-4-displaying

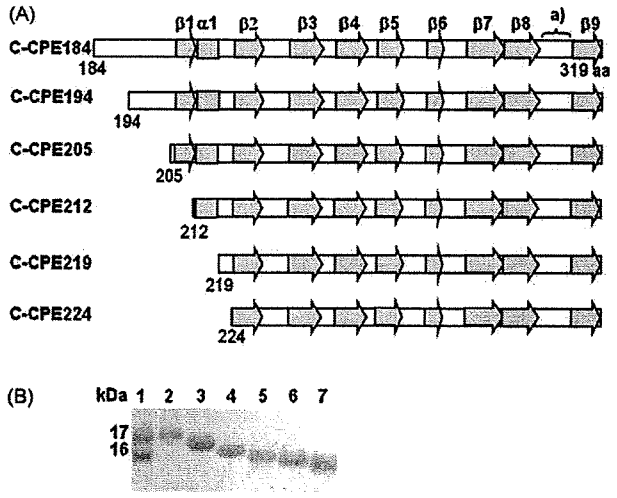

Fig. 2. Preparation of C-CPEs. (A) Schematic structure of C-CPEs. Van Itallie et al. determined the 3-dimensional structure of C-CPE194 containing nine β-sheets and one α-helix [26]. Based on the structural information, we designed five N-terminal truncated C-CPE184 derivatives. (B) CBB staining. C-CPEs were prepared and then purified by affinity chromatography. Lane 1, a maker for molecular weight; lane 2, C-CPE184; lane 3, C-CPE194; lane 4, C-CPE205; lane 5, C-CPE212; lane 6, C-CPE219; lane 7, C-CPE224.

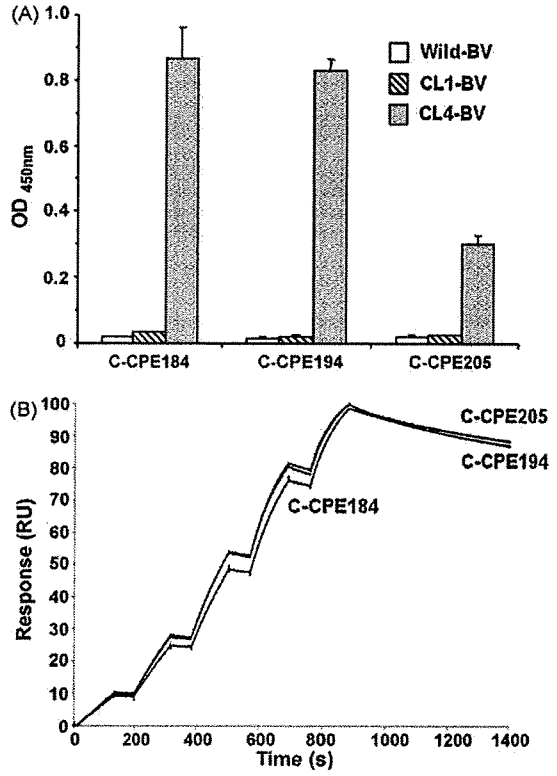

Fig. 3. Interaction of C-CPEs with claudin. (A) ELISA. The immunoplate was coated with wild-type BV (Wild-BV), claudin-1-displaying BV (CL1-BV) or claudin-4-displaying BV (CL4-BV), and then C-CPEs were added to the well. C-CPEs bound to BVs were detected by the addition of anti-his tag antibody and a labeled secondary antibody. Data are means ± SD (n = 3). (B) SPR assay. Claudin-4 was immobilized on a CM5 sensor chip by the amine-coupling method. C-CPEs were injected sequentially at concentrations of 1.25, 2.5, 5, 10 and 20 nM. The association phase was monitored for 120 s at a flow rate of 10 μl/min, and the dissociation phase was followed for 600 s at the same flow rate. The maximum values of response (Rmax) for all curves were compensated to 100 RU.

Table 3
Binding kinetics of C-CPEs to claudin-4.

Derivatives	k_a (l/Ms)	k_d (l/s)	K_D
C-CPE184	5.96×10^5	2.55×10^{-4}	429 pM
C-CPE194	7.13×10^5	3.24×10^{-4}	455 pM
C-CPE205	7.67×10^5	2.87×10^{-4}	374 pM

BV-adsorbed immunoplates, C-CPE194 and C-CPE205 bound to claudin-4-displaying BV but not mock BV or claudin-1-displaying BV (Fig. 3A). We performed SPR analysis to compare the affinities of C-CPEs to claudin-4. Claudin-4 proteins were fixed on the sensor chip, and C-CPEs were injected. Then, we measured the interaction between claudin-4 and C-CPEs. As shown in Fig. 3B and Table 3, C-CPE184, C-CPE194 and C-CPE205 had almost the same affinity to claudin-4 with K_D values of 429, 455 and 374 pM, respectively. The association and dissociation rates of C-CPE194 and C-CPE205 were also similar to those of C-CPE184. C-CPE184, C-CPE194 and C-CPE205 showed similar TJ-modulating activities in Caco-2 monolayer cells; their EC50 values were 0.49, 0.57 and 0.51 μg/ml, respectively (Fig. 4A and Table 4). We performed in situ loop assays to examine the jejunal absorption of FD-4 by C-CPEs. C-CPE194 and C-CPE205 enhanced the jejunal absorption of FD-4 similar to C-CPE184 at 0.2 mg/ml (Fig. 4B–D). Treatment with C-CPE194 or C-CPE205 at 1.0 mg/ml yielded a greater and earlier absorption of FD-4 than treatment at 0.2 mg/ml (Fig. 4B, C). We could not test 1.0 mg/ml of C-CPE184 due to its low solubility.

3.4. Jejunal and pulmonary absorption of hPTH(1-34) by co-treatment with C-CPE194

C-CPE194 enhanced the jejunal absorption of FD-4 to a similar extent as C-CPE184 and C-CPE205; C-CPE194 was also 30- and 3-fold more soluble than C-CPE184 and C-CPE205, respectively. C-CPE194 enhanced the jejunal absorption of hPTH(1-34) at 0.2 and 4.0 mg/ml (Fig. 5A). The AUC values were increased 11.0- and 18.4-fold as compared to the vehicle-treated group (Fig. 5B), and the Cmax and BA of the jejunal absorption of hPTH(1-34) were also increased by C-CPE194 (Table 5). Additionally, the pulmonary absorption of hPTH(1-34) was enhanced by C-CPE194 (AUC = 3080.0 ± 1994.3 ng·min/ml in vechicle-treated group, AUC = 13,397.7 ± 5830.1 ng·min/ml in C-CPE194 (0.8 mg/ml)-treated group) (Fig. 5C, D). The Cmax and BA of hPTH(1-34) were also increased by C-CPE194 (Table 5).

4. Discussion

Biologics are generally hydrophilic and poorly absorbed by the mucosa; therefore, many biologics are administered via injection. The development of a delivery system to allow biologics to pass across the epithelial barrier in mucosa is a pivotal issue for pharmaceutical therapy with biologics, since mucosal administration is needle-free, non-invasive, convenient and comfortable for patients [30,31]. We previously found that C-CPE184 enhanced jejunal absorption of dextran with a molecular mass of <10 kDa through its modulation of the claudin-4 barrier [21]. In the present study, we investigated the effect of a claudin-4 modulator on the mucosal absorption of a biologic, hPTH(1-34), and we found that a claudin-4 modulator is also a potent jejunal, nasal and pulmonary absorption enhancer of this biologic.

CPE is a 35-kDa polypeptide consisting of 319 amino acids [32]. The functional domain of CPE is divided into an N-terminal toxic domain and a C-terminal receptor-binding domain [33]. The receptor-binding fragments of CPE correspond to amino acids 169–319, 171–319, 184–319, 194–319 and 290–319 [20,26,33–35]. Among these fragments, only C-CPE184 and C-CPE194 have been

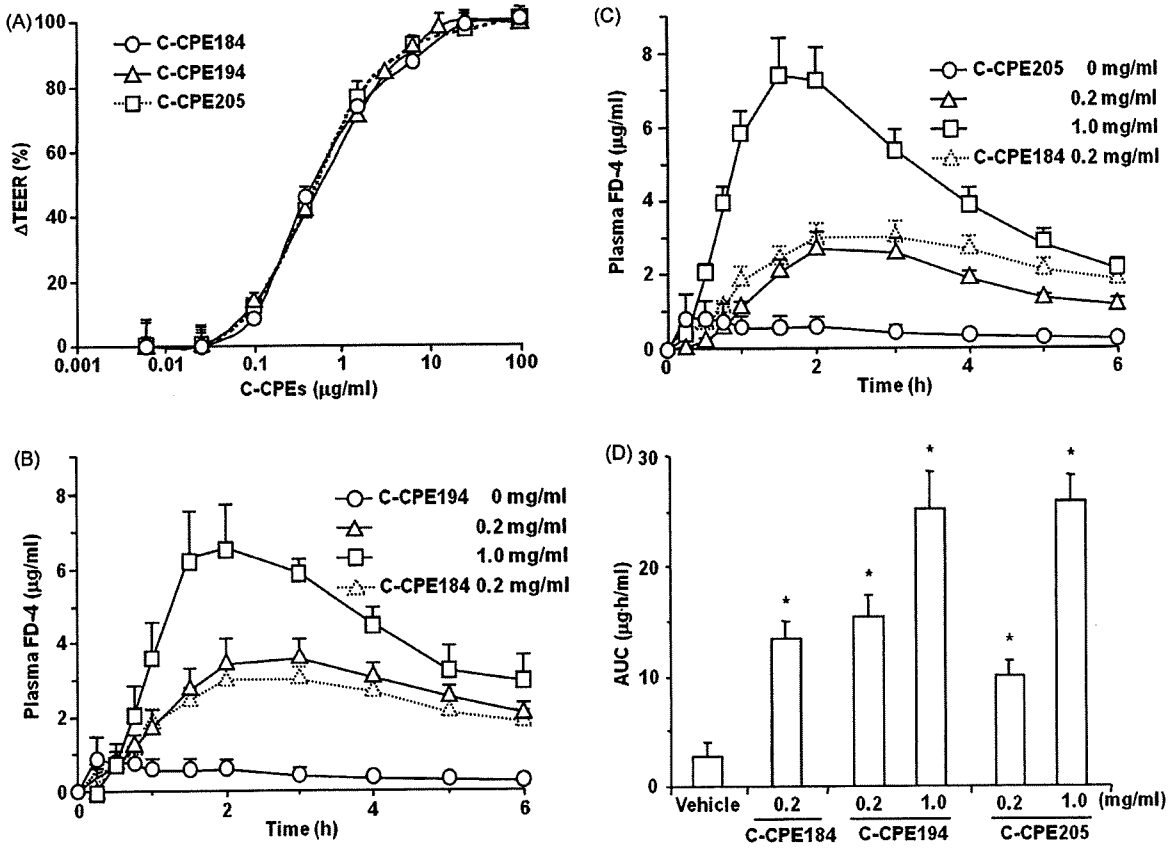

Fig. 4. Modulation of the TJ-barrier by C-CPEs. (A) Caco-2 cells were seeded on a BioCoat™. When TJ-barriers were developed and the cell sheets reached a plateau in their TEER value, C-CPEs were added to the wells from the basal side at the indicated concentration. After 18 h, the TEER was measured. The ΔTEER was calculated as the ratio to reduced TEER values at 0 and 100 μg/ml of C-CPE184 as 0% and 100%, respectively. Data are mean ± SD ($n = 3$). (B–D) Jejunal absorption of FD-4. Jejunum were treated with FD-4 and C-CPEs at the indicated concentration. Time-course changes in plasma FD-4 levels (B, C) and AUC from 0 to 6 h (D). Data are means ± SE ($n = 4$–9). *Significantly different from the vehicle-treated group ($p < 0.05$).

proven to bind to claudin-4 [10,26], and a mucosal-absorption-enhancing effect was proven only for C-CPE184 [21]. The claudin-4 modulator C-CPE184 is a 400-fold more potent jejunal absorption enhancer of dextran as compared to a clinically used absorption enhancer, sodium caprate [21]. However, the low solubility of C-CPE184 (<0.3 mg/ml in PBS) has limited its applicability. This low solubility may result in the slow onset of TJ opening due to limiting the access of C-CPE184 to claudin. Last year, Van Itallie et al. made a breakthrough by truncating the N-terminal of C-CPE184 by 10 amino acids to yield C-CPE194 [26]. They found that C-CPE194 has affinity to claudin-4 and high solubility (>10 mg/ml); moreover, they determined the 3-dimensional structure of C-CPE194, which contains nine β-sheets and one α-helix, and they suggested that the intervening surface loop spanning region 304–312 (located between the β8 and β9 sheets) may be a claudin-binding domain. Based on the structural data for C-CPE194, we prepared five N-terminal-truncated C-CPE184 derivatives: C-CPE194, C-CPE205, C-CPE212 (without the β1 sheet), C-CPE219 (without the β1 sheet and α helix), and C-CPE224 (without the β1 sheet and α helix). C-CPEs lacking the β1 sheet are soluble in PBS containing 2 M Urea but insoluble in PBS. C-CPE184, C-CPE194 and C-CPE205 have almost the same kinetics parameters for binding to claudin-4 and the same TJ-barrier modulating activity (Table 3, Fig. 4A). Thus, the β1 sheet appears to be critical for maintaining the structure of C-CPE, and the N-terminal region corresponding to amino acids 184–204 may not be involved in claudin-4 binding or TJ-barrier modulation.

Table 4
TJ-modulating activities of C-CPEs in Caco-2 cells.

Derivatives	EC50 values[a]
C-CPE184	0.49 μg/ml
C-CPE194	0.57 μg/ml
C-CPE205	0.51 μg/ml

[a] The concentration of C-CPEs at which a 50% decrease in TEER value was observed in Fig. 4A.

Biologics must escape degradation by mucosal enzymes to be absorbed by the mucosa. C-CPE184 (0.2 mg/ml) did not enhance jejunal or pulmonary absorption of hPTH(1-34). However, when hPTH(1-34) was administered 4 h after treatment with C-CPE184, jejunal, pulmonary and nasal absorption was enhanced. Thus, hPTH(1-34) may be degraded in the jejunal and pulmonary mucosa before the enhancement of its absorption by co-administered C-CPE184. Indeed, another claudin-4 modulator, C-CPE194, which is 30-fold more soluble than C-CPE184, significantly enhanced the jejunal and pulmonary absorption of hPTH(1-34). These findings indicate that modulation of claudin-4 may be a potent strategy for mucosal-absorption enhancement of biologics.

Meanwhile, a critical issue in the clinical application of the claudin-4 modulator as a mucosal-absorption enhancer is its safety. Problems with the safety of a claudin-4 modulator include the safety of a claudin-4 modulator in itself and the safety of the modulation of claudin-4, i.e., entry of unwanted substances by the

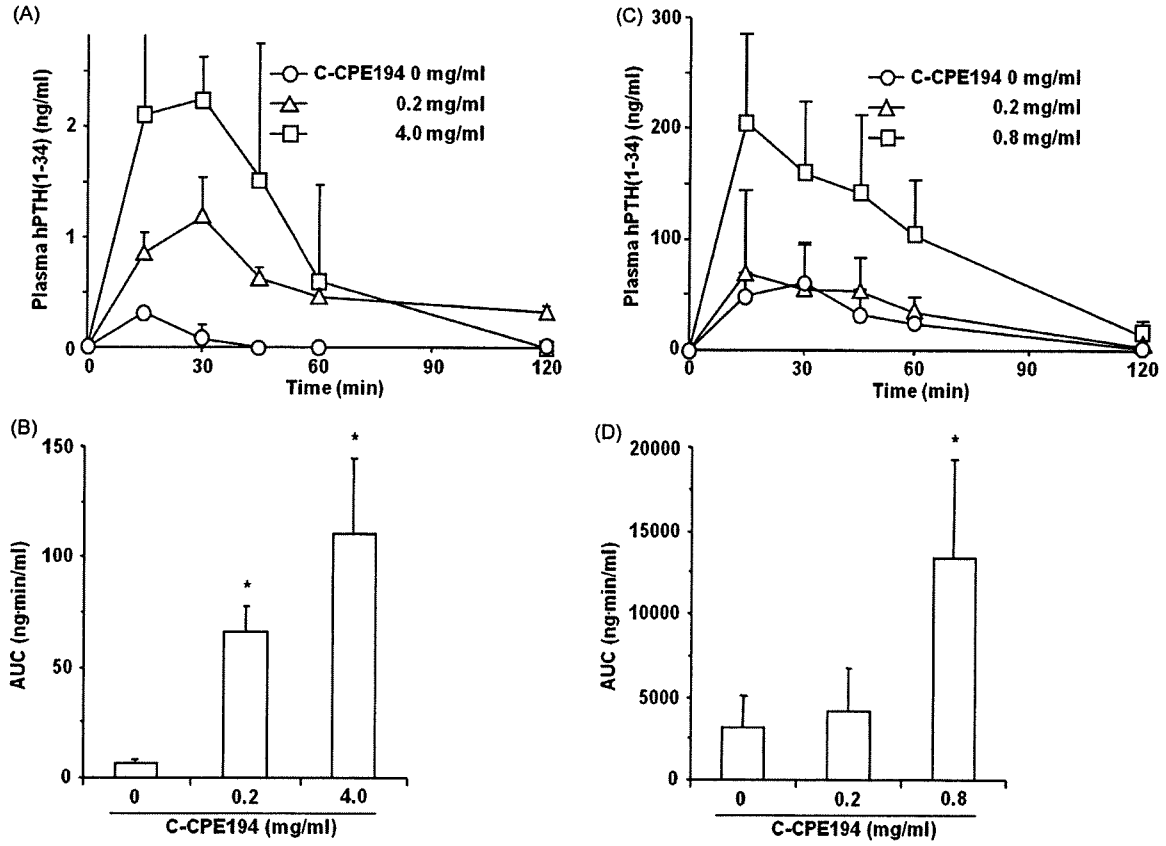

Fig. 5. Mucosal absorption of hPTH(1-34) by a claudin-4 modulator. (A, B) Jejunal absorption of hPTH(1-34). Rat jejunum was treated with hPTH(1-34) (100 μg) and C-CPE194 at the indicated doses. Time-course changes in plasma hPTH(1-34) (A) and AUC from 0 to 120 min (B) were analyzed. (C, D) Pulmonary absorption of hPTH(1-34). hPTH(1-34) (150 μg) and C-CPE194 at the indicated doses were pulmonary administered, and time-course changes in plasma hPTH(1-34) concentration (C) and AUC from 0 to 120 min (D) were analyzed. Data are mean ± SE ($n = 3$). *Significantly different from the vehicle-treated group ($p < 0.05$).

opening of TJs. As mentioned above, C-CPEs are the only claudin-4 modulator. C-CPEs are polypeptide fragments of CPE consisting of more than 120 amino acids, and C-CPEs themselves may have antigenicity. Claudin-4 modulator significantly enhanced jejunal absorption of dextran with a molecular mass of less than 10 kDa [21], and C-CPEs (>14.2 kDa) may not be absorbed by the modulation of claudin-4. Moreover, *C. perfringens* are indigenous bacterium, and immunological tolerance may be induced. Thus, the antigenicity of C-CPE might be partly negligible. Because absorption enhancers would be used as an additive in drugs, they would be repeatedly administered. To avoid the risk of antigenicity, the development of a chemical compound-type or a 30–40 mer peptide-type of claudin modulator is needed. The determination of the 3-dimensional structure of claudin is also important for the theoretical development of promising claudin modulators. Ling et al. prepared a 12-mer peptide-type claudin-4 binder which did not modulate TJs [36], and Van Itallie et al. determined the structure of C-CPE [26]. A peptide-type claudin modulator will be developed in the near future.

The other safety issue is the possible influx of unwanted substances that could be caused by the opening of TJs. C-CPE has demonstrated no damages to mucosal epithelial tissue in rat intestine [21]. Treatment of cells with C-CPE decreased the level of intracellular claudin-4 proteins paralleled by a disruption of the TJ-barrier [10]. Claudin contains the clathrin-sorting signal in its C-terminal intracellular domain, and claudin was often internalized [37,38]. Taken together, these results indicate that C-CPEs may disrupt the TJ-barrier, allowing the movement of solutes through the paracellular route. Do claudin modulators reversibly modulate the TJ-barrier and specifically regulate the movement of solutes? Disruption of the TJ-barrier by C-CPE is reversible, and the TJ-barrier gradually recovered after the removal of C-CPE [10]. The

Table 5
Parameters of mucosal absorption of hPTH(1-34) in C-CPE 194-treated rats.

C-CPE194 (mg/ml)	Jejunum		C-CPE194 (mg/ml)	Pulmonary	
	Cmax (ng/ml)	BA (%)[a]		Cmax (ng/ml)	BA (%)
0	0.3 ± 0.0	0.1 ± 0.0	0	62.3 ± 32.8	26.5 ± 17.4
0.2	1.2 ± 0.4*	0.8 ± 0.2**	0.2	78.7 ± 66.1	34.1 ± 21.6
4.0	2.8 ± 0.2*	1.3 ± 0.3**	0.8	205.2 ± 79.4*	100.6 ± 39.3*

[a] BA (%) = (AUC/Dose)/(AUC iv/Dose iv).
Data are mean ± SE.
*$p < 0.05$, **$p < 0.01$ as compared to the vehicle-treated group.

quick recovery of TJ-barriers will need to be facilitated. One approach is the development of a quickly reversible claudin modulator. Another approach is the development of a claudin inducer for the combination of a claudin modulator and inducer. Another approach is the reduction of unwanted transport using the properties of claudins. Claudin comprises a multigene family consisting of 24 members. Claudin forms paired TJ strands by polymerization in a homomeric and heteromeric manner, and the claudin strands interact in a homotypic and heterotypic manner between adjacent cells [39,40]. TJ-barrier properties are believed to be determined by the combination and mixing ratios of claudin species [41]. Interestingly, the diversity of claudin may contribute to the regulation of specific solute movement through the paracellular route [17]. The expression profiles of claudin in mucosal epithelium exhibit heterogeneity [13–15,42]. The development of claudin modulators with solute and tissue specificity will reduce the non-specific influx of solutes caused by the modulation of TJs.

In summary, we found that claudin-4 modulator enhanced the jejunal, pulmonary and nasal absorption of a peptide drug. This report is the first to indicate that a claudin-4 modulator may be a mucosal-absorption enhancer of biologics.

Acknowledgments

We thank M. Hoshino (Asubio Pharma), N. Kumagai (Asubio Pharma), K. Takashiba (Asubio Pharma), R. Okude (Osaka University) and Y. Nakano (GE Healthcare, Japan) for their excellent technical assistance. We also thank Drs Y. Horiguchi (Osaka University) and M. Furuse (Kobe University) for providing us C-CPE cDNA and claudin cDNA, respectively. This work was supported by a Grant-in-Aid for Scientific Research (21689006) from the Ministry of Education, Culture, Sports, Science and Technology, Japan, by a Health and Labor Sciences Research Grants from the Ministry of Health, Labor and Welfare of Japan and by a grant from Kansai Biomedical Cluster project in Saito, which is promoted by the Knowledge Cluster Initiative of the Ministry of Education, Culture, Sports, Science and Technology, Japan.

References

[1] Powell DW. Barrier function of epithelia. Am J Physiol 1981;241:G275–88.
[2] Engel RH, Riggi SJ. Effect of sulfated and sulfonated surfactants on the intestinal absorption of heparin. Proc Soc Exp Biol Med 1969;130:879–84.
[3] Tidball CS, Lipman RI. Enhancement of jejunal absorption of heparinoid by sodium ethylenediaminetetraacetate in the dog. Proc Soc Exp Biol Med 1962;111:713–5.
[4] Aungst BJ. Intestinal permeation enhancers. J Pharm Sci 2000;89:429–42.
[5] Deli MA. Potential use of tight junction modulators to reversibly open membranous barriers and improve drug delivery. Biochim Biophys Acta 2009;1788:892–910.
[6] Matsuhisa K, Kondoh M, Takahashi A, Yagi K. Tight junction modulator and drug delivery. Expert Opin Drug Deliv 2009;6:509–15.
[7] Kondoh M, Yoshida T, Kakutani H, Yagi K. Targeting tight junction proteins-significance for drug development. Drug Discov Today 2008;13:180–6.
[8] Furuse M, Hirase T, Itoh M, Nagafuchi A, Yonemura S, Tsukita S, et al. Occludin: a novel integral membrane protein localizing at tight junctions. J Cell Biol 1993;123:1777–88.
[9] Furuse M, Fujita K, Hiiragi T, Fujimoto K, Tsukita S. Claudin-1 and -2: novel integral membrane proteins localizing at tight junctions with no sequence similarity to occludin. J Cell Biol 1998;141:1539–50.
[10] Sonoda N, Furuse M, Sasaki H, Yonemura S, Katahira J, Horiguchi Y, et al. *Clostridium perfringens* enterotoxin fragment removes specific claudins from tight junction strands: evidence for direct involvement of claudins in tight junction barrier. J Cell Biol 1999;147:195–204.
[11] Furuse M, Hata M, Furuse K, Yoshida Y, Haratake A, Sugitani Y, et al. Claudin-based tight junctions are crucial for the mammalian epidermal barrier: a lesson from claudin-1-deficient mice. J Cell Biol 2002;156:1099–111.
[12] Nitta T, Hata M, Gotoh S, Seo Y, Sasaki H, Hashimoto N, et al. Size-selective loosening of the blood-brain barrier in claudin-5-deficient mice. J Cell Biol 2003;161:653–60.
[13] Rahner C, Mitic LL, Anderson JM. Heterogeneity in expression and subcellular localization of claudins 2, 3, 4, and 5 in the rat liver, pancreas, and gut. Gastroenterology 2001;120:411–22.
[14] Takano K, Kojima T, Go M, Murata M, Ichimiya S, Himi T, et al. HLA-DR- and CD11c-positive dendritic cells penetrate beyond well-developed epithelial tight junctions in human nasal mucosa of allergic rhinitis. J Histochem Cytochem 2005;53:611–9.
[15] Wang F, Daugherty B, Keise LL, Wei Z, Foley JP, Savani RC, et al. Heterogeneity of claudin expression by alveolar epithelial cells. Am J Respir Cell Mol Biol 2003;29:62–70.
[16] Krause G, Winkler L, Mueller SL, Haseloff RF, Piontek J, Blasig IE. Structure and function of claudins. Biochim Biophys Acta 2008;1778:631–45.
[17] Krause G, Winkler L, Piehl C, Blasig I, Piontek J, Muller SL. Structure and function of extracellular claudin domains. Ann N Y Acad Sci 2009;1165:34–43.
[18] McClane BA, Hanna PC, Wnek AP. *Clostridium perfringens* enterotoxin. Microb Pathog 1988;4:317–23.
[19] Fujita K, Katahira J, Horiguchi Y, Sonoda N, Furuse M, Tsukita S. *Clostridium perfringens* enterotoxin binds to the second extracellular loop of claudin-3, a tight junction integral membrane protein. FEBS Lett 2000;476:258–61.
[20] Katahira J, Inoue N, Horiguchi Y, Matsuda M, Sugimoto N. Molecular cloning and functional characterization of the receptor for *Clostridium perfringens* enterotoxin. J Cell Biol 1997;136:1239–47.
[21] Kondoh M, Masuyama A, Takahashi A, Asano N, Mizuguchi H, Koizumi N, et al. A novel strategy for the enhancement of drug absorption using a claudin modulator. Mol Pharmacol 2005;67:749–56.
[22] Wray C, Mao Y, Pan J, Chandrasena A, Piasta F, Frank JA. Claudin-4 augments alveolar epithelial barrier function and is induced in acute lung injury. Am J Physiol Lung Cell Mol Physiol 2009;297:L219–27.
[23] Suzuki Y, Yabuta M, Ohsuye K. High-level production of recombinant human parathyroid hormone 1-34. Appl Environ Microbiol 1998;64:526–9.
[24] Saeki R, Kondoh M, Kakutani H, Tsunoda SI, Mochizuki Y, Hamakubo T, et al. A novel tumor-targeted therapy using a claudin-4-targeting molecule. Mol Pharmacol 2009;76:918–26.
[25] Mitic LL, Unger VM, Anderson JM. Expression, solubilization, and biochemical characterization of the tight junction transmembrane protein claudin-4. Protein Sci 2003;12:218–27.
[26] Van Itallie CM, Betts L, Smedley 3rd JG, McClane BA, Anderson JM. Structure of the claudin-binding domain of *Clostridium perfringens* enterotoxin. J Biol Chem 2008;283:268–74.
[27] Karlsson R, Katsamba PS, Nordin H, Pol E, Myszka DG. Analyzing a kinetic titration series using affinity biosensors. Anal Biochem 2006;349:136–47.
[28] Myszka DG. Improving biosensor analysis. J Mol Recognit 1999;12:279–84.
[29] Takahashi A, Komiya E, Kakutani H, Yoshida T, Fujii M, Horiguchi Y, et al. Domain mapping of a claudin-4 modulator, the C-terminal region of C-terminal fragment of *Clostridium perfringens* enterotoxin, by site-directed mutagenesis. Biochem Pharmacol 2008;75:1639–48.
[30] Sayani AP, Chien YW. Systemic delivery of peptides and proteins across absorptive mucosae. Crit Rev Ther Drug Carrier Syst 1996;13:85–184.
[31] Song Y, Wang Y, Thakur R, Meidan VM, Michniak B. Mucosal drug delivery: membranes, methodologies, and applications. Crit Rev Ther Drug Carrier Syst 2004;21:195–256.
[32] Czeczulin JR, Hanna PC, McClane BA. Cloning, nucleotide sequencing, and expression of the *Clostridium perfringens* enterotoxin gene in *Escherichia coli*. Infect Immun 1993;61:3429–39.
[33] Hanna PC, Wieckowski EU, Mietzner TA, McClane BA. Mapping of functional regions of *Clostridium perfringens* type A enterotoxin. Infect Immun 1992;60:2110–4.
[34] Hanna PC, Mietzner TA, Schoolnik GK, McClane BA. Localization of the receptor-binding region of *Clostridium perfringens* enterotoxin utilizing cloned toxin fragments and synthetic peptides. The 30 C-terminal amino acids define a functional binding region. J Biol Chem 1991;266:11037–43.
[35] Kokai-Kun JF, McClane BA. Deletion analysis of the *Clostridium perfringens* enterotoxin. Infect Immun 1997;65:1014–22.
[36] Ling J, Liao H, Clark R, Wong MS, Lo DD. Structural constraints for the binding of short peptides to claudin-4 revealed by surface plasmon resonance. J Biol Chem 2008;283:30585–9.
[37] Ivanov AI, Nusrat A, Parkos CA. Endocytosis of epithelial apical junctional proteins by a clathrin-mediated pathway into a unique storage compartment. Mol Biol Cell 2004;15:176–88.
[38] Matsuda M, Kubo A, Furuse M, Tsukita S. A peculiar internalization of claudins, tight junction-specific adhesion molecules, during the intercellular movement of epithelial cells. J Cell Sci 2004;117:1247–57.
[39] Furuse M, Furuse K, Sasaki H, Tsukita S. Conversion of zonulae occludentes from tight to leaky strand type by introducing claudin-2 into Madin-Darby canine kidney I cells. J Cell Biol 2001;153:263–72.
[40] Furuse M, Sasaki H, Tsukita S. Manner of interaction of heterogeneous claudin species within and between tight junction strands. J Cell Biol 1999;147:891–903.
[41] Furuse M, Tsukita S. Claudins in occluding junctions of humans and flies. Trends Cell Biol 2006;16:181–8.
[42] Coyne CB, Gambling TM, Boucher RC, Carson JL, Johnson LG. Role of claudin interactions in airway tight junctional permeability. Am J Physiol Lung Cell Mol Physiol 2003;285:L1166–78.

Biomaterials xxx (2010) 1–9

Contents lists available at ScienceDirect

Biomaterials

journal homepage: www.elsevier.com/locate/biomaterials

Mucosal vaccination using claudin-4-targeting

Hideki Kakutani [a], Masuo Kondoh [a,*], Masahiro Fukasaka [a], Hidehiko Suzuki [a], Takao Hamakubo [b], Kiyohito Yagi [a,**]

[a] Laboratory of Bio-Functional Molecular Chemistry, Graduate School of Pharmaceutical Sciences, Osaka University, Suita, Osaka 565-0871, Japan
[b] Department of Molecular Biology and Medicine, Research Center for Advanced Science and Technology, The University of Tokyo, Meguro, Tokyo 153-8904, Japan

ARTICLE INFO

Article history:
Received 12 January 2010
Accepted 19 March 2010
Available online xxx

Keywords:
Immunomodulation
Mucosa
Drug delivery
Epithelium

ABSTRACT

Mucosa-associated lymphoid tissue (MALT) plays pivotal roles in mucosal immune responses. Efficient delivery of antigens to MALT is a critical issue for the development of mucosal vaccines. Although claudin-4 is preferentially expressed in MALT in the gut, a claudin-4-targeting approach for mucosal vaccination has never been developed. In the present study, we found that claudin-4 is expressed in nasal MALT, and we prepared a fusion protein of ovalbumin (OVA) as a model antigen with a claudin-4-binder, the C-terminal fragment of *Clostridium perfringens* enterotoxin (C-CPE) (OVA-C-CPE). Nasal immunization with OVA-C-CPE, but not a mixture of OVA and C-CPE, induced the production of OVA-specific serum IgG and nasal, vaginal and fecal IgA. Deletion of the claudin-4-binding region in OVA-C-CPE attenuated the induction of the immune responses. OVA-C-CPE immunization activated both Th1 and Th2 responses, and nasal immunization with OVA-C-CPE showed anti-tumor activity in mice inoculated with OVA-expressing thymoma cells. These results indicate that the claudin-4-targeting may be a potent strategy for nasal vaccination.

1. Introduction

Each year, 17 million people die from infectious diseases worldwide, and 7 million people die from cancers worldwide (http://www.globalhealth.org/infectious_diseases/; http://www.reuters.com/article/healthNews/idUSN1633064920071217). Thus, the development of methods to prevent and treat infectious diseases and cancers is an important issue for healthcare worldwide. Vaccination against these diseases is a promising approach because of its low frequency of side effects and its great preventative and therapeutic effects. Vaccination strategies are classified as parenteral or mucosal.

Parenteral vaccination is effective for the elimination of infectious cells and cancer cells by the induction of systemic immune responses. Parenteral vaccines are administered by injections, which are invasive, painful, and have low levels of patient compliance; moreover, mucosal immunological defense is not induced. In contrast, mucosal vaccine elicits both mucosal and systemic immune responses, resulting in the prevention of infection on the mucosal surfaces and the elimination of pathological cells [1–3]. Mucosal administration is needle-free, less painful, and has improved patience compliance. Thus, mucosal vaccination appears to be an ideal vaccination strategy, although mucosally administered protein antigens are poorly immunogenic. Various approaches for the mucosal delivery of antigens have been investigated [4–6]. Mucosa-associated lymphoid tissues (MALTs) play pivotal roles in mucosal immunological responses [7,8]. MALTs comprise gut-associated lymphoid tissues (GALT), nasopharynx-associated lymphoid tissue (NALT) and bronchus-associated lymphoid tissue (BALT). MALT contains lymphocytes, M cells, T cells, B cells and antigen-presenting cells (APCs), and the efficient delivery of antigens into MALT is essential for mucosal vaccinations [9]. Indeed, there have been several attempts to deliver antigens to MALT using microparticles, liposomes, saponins or chitosans [4–6].

Immunization at one mucosal surface can generate secretory IgA responses at other mucosal sites. Ideally, vaccination at a single site would provide both humoral and cell-mediated protection, not only

Abbreviations: MALT, mucosa-associated lymphoid tissue; OVA, ovalbumin; C-CPE, C-terminal fragment of *Clostridium perfringens* enterotoxin; OVA-C-CPE, fusion proteins of OVA and C-CPE; GALT, gut-associated lymphoid tissue; NALT, nasopharynx-associated lymphoid tissue; BALT, bronchus-associated lymphoid tissue; APC, antigen-presenting cell; FAE, follicle-associated epithelium; TJ, tight junction; CPE, *Clostridium perfringens* enterotoxin; RT-PCR, reverse transcriptase-polymerase chain reaction; SDS-PAGE, sodium dodecyl sulfate-polyacrylamide gel electrophoresis; PBS, phosphate-buffered saline; ELISA, enzyme-linked immunosorbent assay; BV, budded baculovirus; FBS, fetal bovine serum; TBS, tris-buffered saline; IFN, interferon; IL, interleukin.

* Corresponding author. Tel.: +81 6 6879 8196; fax: +81 6 6879 8199.
** Corresponding author. Tel./fax: +81 6 6879 8195.
E-mail addresses: masuo@phs.osaka-u.ac.jp (M. Kondoh), yagi@phs.osaka-u.ac.jp (K. Yagi).

0142-9612/$ – see front matter © 2010 Published by Elsevier Ltd.
doi:10.1016/j.biomaterials.2010.03.047

at the relevant mucosal surface, but also throughout the body [4]. In this regard, nasal vaccination has shown particular potential. Nasally administered vaccines induced mucosal IgA antibody responses in the salivary glands, respiratory tracts, genital tracts, and intestines [10–12]. The nasal route can also induce cytotoxic T lymphocytes in distant mucosal tissues including the female genital tract [13]. Additionally, nasal immunization produced greater systemic antibody responses than other mucosal immunization routes [12,14]. However, despite these encouraging characteristics, free antigens are usually unable to stimulate immune responses following intranasal administration due to their ineffective delivery to immune response-inducing sites [15]. Thus, the effective delivery of antigens to NALT is needed for the development of a potent nasal vaccine.

A single layer of epithelial cell sheet follicle-associated epithelium (FAE) covers NALT. FAE contains M cells, which are key antigen-sampling cells for the delivery of mucosally encountered antigens to the underlying APCs, and FAE plays a pivotal role in the mucosal immunological response [16–18]. Antigen delivery using a ligand for the FAE that covers NALT would be a potent strategy for the development of a mucosal vaccine. Epithelium has well-developed tight junctions (TJs) that seal the intercellular space on the epithelial cell sheets [19,20]. Occludin, claudin and junctional adhesion molecule are components of TJs [21]. Among these components, claudin-4 was preferentially expressed on the dome region of FAE in GALT [22]. We found that claudin-4 was also expressed in NALT (Fig. 1). These findings strongly indicate that claudin-4-targeting may be useful for mucosal vaccines; however, a mucosal vaccine that uses a claudin-4-binder has never been developed.

Clostridium perfringens enterotoxin (CPE) causes food poisoning in humans [23]. A receptor for CPE is claudin-4, and the C-terminal fragment of CPE (C-CPE) is a claudin-4-binder [24–26]. We previously prepared a claudin-4-targeting cytotoxic molecule by genetically fusing a cytotoxin with C-CPE [27,28]. In the present study, we investigated whether claudin-4-targeting is a potent strategy for mucosal vaccine using C-CPE-fused antigen protein.

2. Materials and methods

2.1. Animals

Female BALB/c mice and C57BL/6 mice (6–8 weeks old) were purchased from SLC, Inc. (Shizuoka, Japan). The mice were housed at 23 ± 1.5 °C with a 12-h light/dark cycle and were allowed free access to standard rodent chow and water. After their arrival, the mice were allowed to adapt to their environment for at least 1 week before the experiments. The animal experiments were performed according to the guidelines of Osaka University.

2.2. Reverse transcriptase-polymerase chain reaction (RT-PCR)

Total mRNA was extracted from NALT using Isogen (Nippongene, Toyama, Japan), and the mRNA was reverse-transcribed using an RNA PCR kit (AMV, Ver.3.0) according to the manufacturer's instructions (Takara, Kyoto, Japan). The polymerase chain reaction (PCR) amplification from the resultant cDNA was performed using primer pairs for claudin-4 (forward, 5′-tggatgaactgcgtggtg-3′; reverse, 5′-ggttgtagaagtcgcggatg-3′) for 35 reaction cycles (94 °C, 45 s; 52 °C, 60 s; 72 °C, 30 s) or β-actin (forward, 5′-tagatgggcacagtgtggg-3′; reverse, 5′-ggcgtgatggtgggcatgg-3′) for 30 reaction cycles (94 °C, 30 s; 58 °C, 60 s; 72 °C, 30 s). The amplified products were separated by electrophoresis on a 2% agarose gel and visualized with ethidium bromide.

2.3. Immunoblotting for claudin-4

NALT was lysed in a lysis buffer (50 mM Tris–HCl, pH 7.5, 0.15 M NaCl, 0.1% Triton X-100, 0.1% SDS, 1 mM sodium orthovanadate, 1 mM EDTA, 1 mM NaF, and 1 mM phenylmethylsulfonyl fluoride). The lysates (10 μg of protein) were subjected to sodium dodecyl sulfate-polyacrylamide gel electrophoresis (SDS-PAGE) followed by western blotting with anti-claudin-4 (Zymed Laboratory, South San Francisco, CA) or anti-β-actin antibodies (Sigma–Aldrich, St. Louis, MO). The immunoreactive bands were detected with a peroxidase-labeled secondary antibody followed by visualization with a chemiluminescence reagent (Amersham Bioscience, Piscataway, NJ).

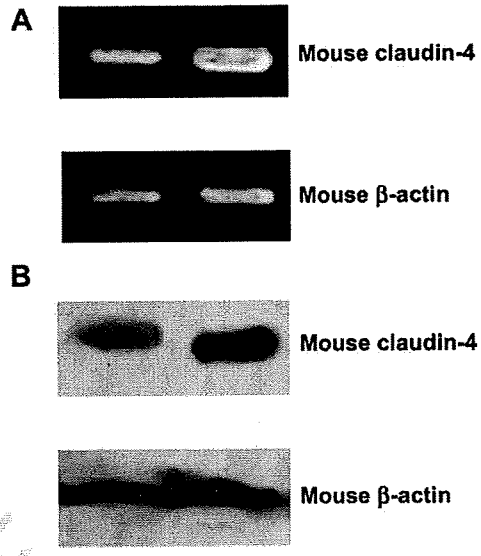

Fig. 1. Expression of claudin-4 in NALT. A) RT-PCR analysis. mRNA was isolated from NALT of mice, and expression of claudin-4 was assayed by RT-PCR. B) Immunoblot analysis. The lysate of NALT was subjected to SDS-PAGE, followed by western blotting with anti-claudin-4 Ab. β-actin was used as an internal control.

2.4. Preparation of OVA-C-CPE fusion proteins

We prepared expression plasmids encoding fusion proteins of OVA with C-CPE or C-CPE303, in which the claudin-4-binding C-terminal 16 amino acids of C-CPE were deleted [29]. Oligonucleotides containing a G4S linker and multiple cloning sites, including KpnI, SpeI, SmaI and PacI sites, were subcloned into NdeI-digested pET16b (Novagen, Darmstadt, Germany), pET-C-CPE and pET-C-CPE303 [30], resulting in pET-MCS and pET-MCS-C-CPEs. OVA cDNA was PCR amplified using pCMV Script/OVA (Kindly provided from Dr. S. Nakagawa, Osaka University, Japan) as a template, a forward primer (5′-gcggtaccatgggctccatcggcgcagc-3′, KpnI site is underlined), and a reverse primer (5′-ccttaattaaaggggaaacacatctgccaa-3′, PacI site is underlined). The resulting OVA fragment was inserted into pET-MCS and pET-MCS-C-CPEs at the KpnI/PacI site, resulting in pET-OVA, pET-OVA-C-CPE and pET-OVA-C-CPE303. The OVA-fusion protein plasmids were transduced into *Escherichia coli* strain BL21 (DE3), and the production of OVA and OVA-C-CPEs was induced by the addition of isopropyl-D-thiogalactopyranoside. The harvested cells were lysed in buffer A (10 mM Tris–HCl, pH 8.0, 400 mM NaCl, 5 mM $MgCl_2$, 0.1 mM PMSF, 1 mM 2-mercaptoethanol, and 10% glycerol) supplemented with 8 M urea when necessary. The lysates were applied to HiTrap™ HP (GE Healthcare, Buckinghamshire, UK), and the fusion proteins were eluted with buffer A containing 100–500 mM imidazole. The solvent was exchanged with phosphate-buffered saline (PBS) using a PD-10 column (GE Healthcare), and the purified protein was stored at −80 °C until use. Purification of the fusion proteins was confirmed by SDS-PAGE, followed by staining with Coomassie Brilliant Blue and by immunoblotting with anti-his-tag antibody. Protein assays were performed using a BCA protein assay kit (Pierce Chemical, Rockford, IL) with bovine serum albumin as a standard.

2.5. Enzyme-linked immunosorbent assay (ELISA)

Budded baculovirus (BV) displaying mouse claudin-1 or -4 was prepared as described previously [28]. Briefly, the DNA fragments of claudin-1 or -4 were subcloned into the baculoviral transfer vector pFastBac1 (Invitrogen, Gaithersburg, MD). Recombinant baculoviruses were generated using the Bac-to-Bac system (Invitrogen). Sf9 cells maintained in Grace's Insect medium containing 10% fetal bovine serum (FBS) at 27 °C were infected with the recombinant baculoviruses. After 70 h, the conditioned medium was recovered and centrifuged. The resultant pellets of the BV fraction were suspended in Tris-buffered saline (TBS) containing protease inhibitor cocktail and then stored at 4 °C until use.

The BV displaying claudins was diluted with TBS and adsorbed to the wells of 96-well ELISA plates (Greiner Bio-One, Tokyo, Japan) overnight at 4 °C. The wells were blocked with TBS containing 1.6% BlockAce (Dainippon Sumitomo Pharmaceutical, Osaka, Japan) for 2 h at room temperature and the C-CPE, OVA-C-CPE or OVA-C-CPE303 was added. After 2-h incubation, the wells were washed and incubated with anti-his-tag antibody followed by a horseradish peroxidase-conjugated secondary antibody. The immunoreactive proteins were detected using TMB peroxidase substrate at an absorbance of 450 nm.

2.6. Nasal immunization

Mice were nasally immunized with 10-μl aliquots of OVA, a mixture of OVA and C-CPE, OVA-C-CPE or OVA-C-CPE303 at the indicated schedules. The doses of the proteins were equal to 5 μg of OVA and 1.89 μg of C-CPE.

2.7. OVA-specific antibody production

Seven days after the last immunization, serum and mucosal secretions (nasal washes, vaginal washes, and fecal extracts) were collected. Fecal pellets (100 mg) were suspended in 1 ml of PBS and extracted by vortexing for 10 min. The samples were centrifuged at 3000×g for 10 min, and the resultant supernatants were used as fecal extracts. Vaginal and nasal mucosa were washed with 100 or 200 μl of PBS, respectively.

The titers of OVA-specific antibody in serum, extracts and mucosal washes were determined by ELISA. Briefly, an immunoplate was coated with OVA (100 μg/well in a 96-well plate). Ten-fold serial dilutions of these samples were added to the immunoplate followed by the addition of horseradish peroxidase-conjugated anti-mouse IgG, IgG1, IgG2a or IgA. The OVA-specific antibodies were detected using TMB peroxide substrate. End-point titers were expressed as the dilution ratio, which gave 0.1 above control values obtained for serum of naïve mice at an absorbance of 450 nm.

2.8. Cytokine ELISA

Serum interferon factor-γ (IFN-γ) and Interleukin-13 (IL-13) were measured with an ELISA kit according to the manufacturer's protocol (R&D Systems, Inc., MN).

2.9. Cell cultures

A murine thymoma cell line EL4 (H-2^b) was cultured in RPMI 1640 supplemented with 10% FBS. EG7-OVA cells (OVA-transfected EL4 cells) were maintained in RPMI 1640 containing 10% FBS in the presence of 400 μg/ml of G418.

2.10. Anti-tumor activity

In an anti-tumor assay, female C57BL/6 mice (6–8 weeks) were nasally immunized with vehicle, OVA, a mixture of OVA and C-CPE, OVA-C-CPE or OVA-C-CPE303 once a week for 3 weeks. All non-vehicle immunizations contained equivalent amounts of OVA (5 μg). Seven days after the last immunization, the mice were subcutaneously inoculated with 1×10^6 EG7-OVA cells. Tumor growth was monitored by measuring two diameters, and the tumor volume was calculated as $a \times b \times b/2$, where a is the maximum diameter of the tumor and b is the minimum diameter of the tumor.

2.11. Statistical analysis

Results were analyzed by an analysis of variance (ANOVA) followed by the Dunnett multiple comparison test, and statistical significance was assigned at $p < 0.05$.

3. Results

3.1. Expression of claudin-4 in NALT

Nasal vaccine is a potent therapy for infectious diseases and cancers since nasal vaccination potentiates humoral and cellular immune responses throughout the body. NALT is the nasal lymphoid tissue, and effective delivery of antigens to NALT is critical for the development of mucosal vaccinations. A previous report showed that claudin-4 is expressed in GALT [22], whereas it is unclear whether claudin-4 is expressed in NALT. To investigate the expression of claudin-4 in NALT, NALT was isolated from mice, and the NALT lysate was subjected to RT-PCR and immunoblotting analyses. As shown in Fig. 1A and B, claudin-4 mRNA and protein were detected in NALT. These data indicate that claudin-4-binder may be a targeting molecule for NALT.

3.2. Preparation of claudin-4-targeting OVA

Claudin has low antigenicity, and there has been little success in the preparation of antibodies against the extracellular region of claudin. C-CPE corresponding to aa 184–319 at the C-terminal of CPE is a claudin-4-binder [24,25]. We previously prepared a claudin-4-targeting cytotoxic molecule genetically fused with C-CPE [27]. To evaluate whether a claudin-4-targeting strategy is an effective method for mucosal vaccination, we genetically fused C-CPE with OVA, a popular model antigen for vaccination, to yield OVA-C-CPE (Fig. 2A). OVA-C-CPE was produced by *E. coli* and purified by affinity chromatography. Purification of the protein was confirmed by SDS-PAGE and immunoblotting (Fig. 2B). The molecular size was identical to the predicted size of 62 kDa for OVA-C-CPE. To evaluate the binding of OVA-C-CPE to claudin-4, we performed ELISA with a claudin-displaying BV-coated immunoplate. OVA-C-CPE or C-CPE was added to wells coated with wild-type BV, claudin-1-BV or claudin-4-BV. The bound proteins were detected using anti-his-tag antibody. Like C-CPE, OVA-C-CPE bound to claudin-4-BV but not wild-type BV or claudin-1-BV (Fig. 2C).

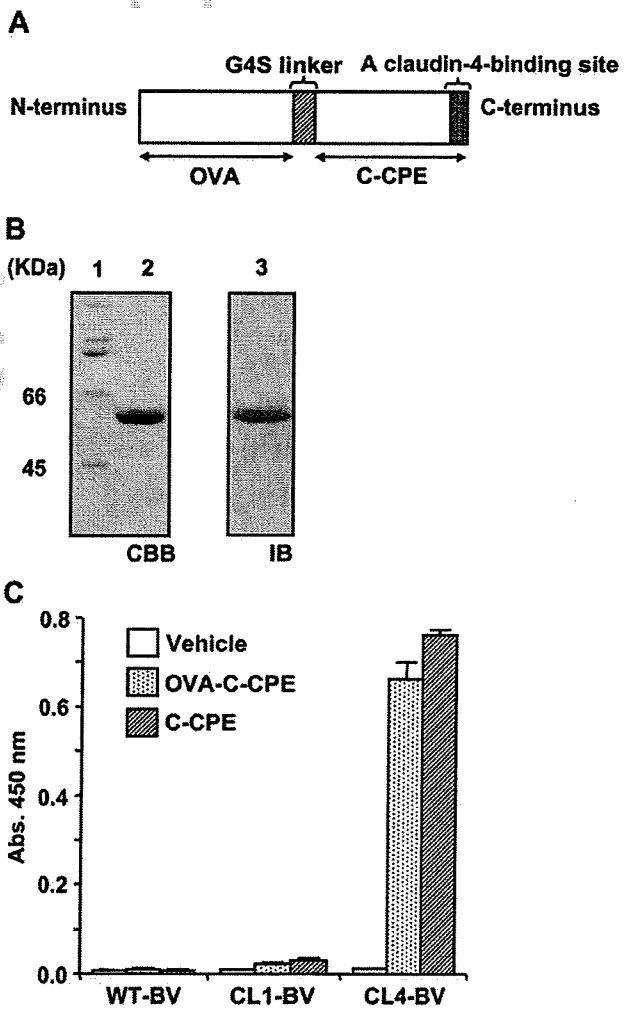

Fig. 2. Preparation of OVA-C-CPE. A) Schematic illustration of OVA-C-CPE. The claudin-4-binding site of C-CPE is located in the C-terminal 16 amino acids [29]. OVA was fused with C-CPE at the N-terminal of C-CPE, resulting in OVA-C-CPE. B) Purification of OVA-C-CPE. OVA-C-CPE was expressed in *E. Coli* as a his-tagged protein and isolated by Ni-affinity chromatography. The purification of OVA-C-CPE was confirmed by SDS-PAGE followed by staining with Coomassie Brilliant Blue (CBB, left panel) and by immunoblotting with an anti-his-tag antibody (IB, right panel). Lane 1: molecular weight marker; lane 2, 3: OVA-C-CPE. The putative molecular mass of OVA-C-CPE is 62 kDa. C) Binding of OVA-C-CPE to claudin-4. Wild-type BV (WT-BV), BV displaying claudin-1 (CL1-BV) or -4 (CL4-BV) was absorbed onto a 96-well immunoplate, and then vehicle, OVA-C-CPE or C-CPE was added to the well. OVA-C-CPE or C-CPE bound to BV was detected by an anti-his-tag Ab followed by horseradish peroxidase-labeled secondary Ab. C-CPE was used as a positive control for a claudin-4-binding. Data are means ± SD ($n = 4$).

3.3. Induction of OVA-specific humoral responses

To clarify whether claudin-4-targeting activates an immune response, we investigated antigen-specific humoral responses at both systemic and mucosal sites in mice that received nasally administered OVA-C-CPE. Mice received an intranasal administration of OVA, a mixture of OVA and C-CPE, or OVA-C-CPE fusion protein once a week for 3 weeks. Seven days after the last administration, we measured the OVA-specific serum IgG, nasal IgA, vaginal IgA and fecal IgA levels. As shown in Fig. 3A, the OVA-specific serum IgG responses were increased in mice immunized with OVA-C-CPE as compared to the mice immunized with OVA or a mixture of OVA and C-CPE. The OVA-specific IgA responses in nasal washes were greater from mice immunized with OVA-C-CPE than from mice immunized with OVA or a mixture of OVA and C-CPE (Fig. 3B). It is a superior character of mucosal vaccination that antigen-specific IgA responses were induced not only at the immunized site but also at remote mucosal surfaces [4]. As shown in Fig. 3C and D, nasal immunization with OVA-C-CPE activated vaginal and fecal OVA-specific IgA responses. The OVA-specific IgA responses did not occur in mice immunized with a mixture of OVA and C-CPE. These data suggest that fusion of OVA with C-CPE is critical for successful nasal vaccination.

We previously found that the C-terminal 16 amino acids of C-CPE are essential for claudin-4-binding [29]. To investigate the involvement of claudin-4 in OVA-specific humoral responses in mice nasally immunized with OVA-C-CPE, we prepared OVA-C-CPE303, in which the claudin-4-binding region was deleted (Fig. 4A). Deletion of the 16 amino acid region attenuated the claudin-4-binding of OVA-C-CPE (Fig. 4B). OVA-specific serum IgG and nasal, vaginal and fecal mucosal IgA responses were also attenuated in mice immunized with OVA-C-CPE303 (Fig. 4C and D, 4E and 4F, respectively). No histological mucosal injury was found after nasal immunization with OVA-C-CPE (data not shown). These findings indicate that claudin-4-targeting may be involved in nasal vaccination by OVA-C-CPE.

3.4. Induction of Th1 and Th2 responses by OVA-C-CPE

Nasal immunization of antigen induced antigen-specific immune responses including Th1- and Th2-type responses [31,32]. We next investigated whether nasal immunization with OVA-C-CPE evoked Th1- or Th2-type responses. The OVA-specific IgG1 (a Th2 response) and IgG2a (a Th1 response) responses in the serum of mice nasally immunized with OVA-C-CPE were significantly enhanced compared to those of mice immunized with OVA alone or a mixture of OVA and C-CPE (Fig. 5A). Measurement of Th1 (IFN-γ) and Th2 (IL-13)-specific cytokines in splenocytes isolated from mice nasally immunized with OVA, a mixture of OVA and C-CPE, or OVA-C-CPE showed that nasal immunization with OVA-C-CPE increased both Th1 and Th2 cytokine production (Fig. 5B). Th1 and

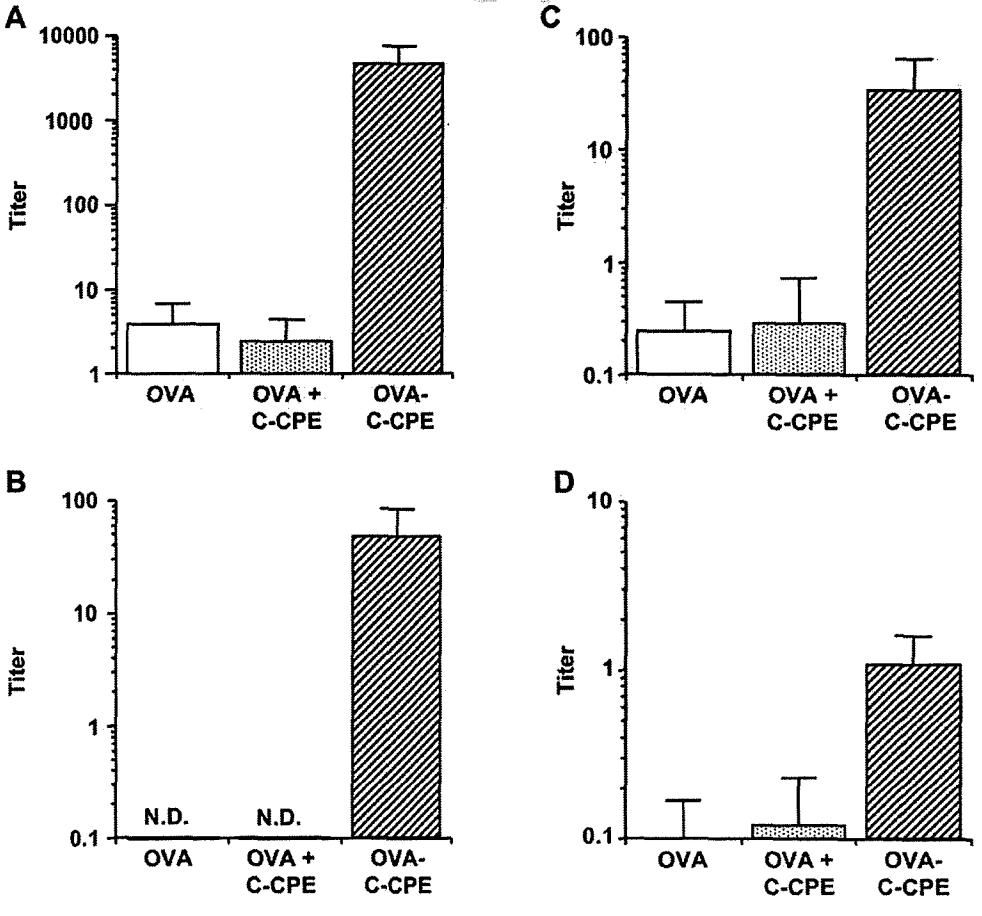

Fig. 3. Production of OVA-specific IgG and IgA by OVA-C-CPE. Mice were nasally immunized with vehicle, OVA, a mixture of OVA and C-CPE, or OVA-C-CPE (5 μg OVA) once a week for 3 weeks. Seven days after the last immunization, the levels of serum IgG (A), nasal IgA (B), vaginal IgA (C) and fecal IgA (D) were determined by ELISA. Data are means ± SD ($n = 4$). The results are representative of three independent experiments. N.D., not detected.

Please cite this article in press as: Kakutani H, et al., Mucosal vaccination using claudin-4-targeting, Biomaterials (2010), doi:10.1016/j.biomaterials.2010.03.047

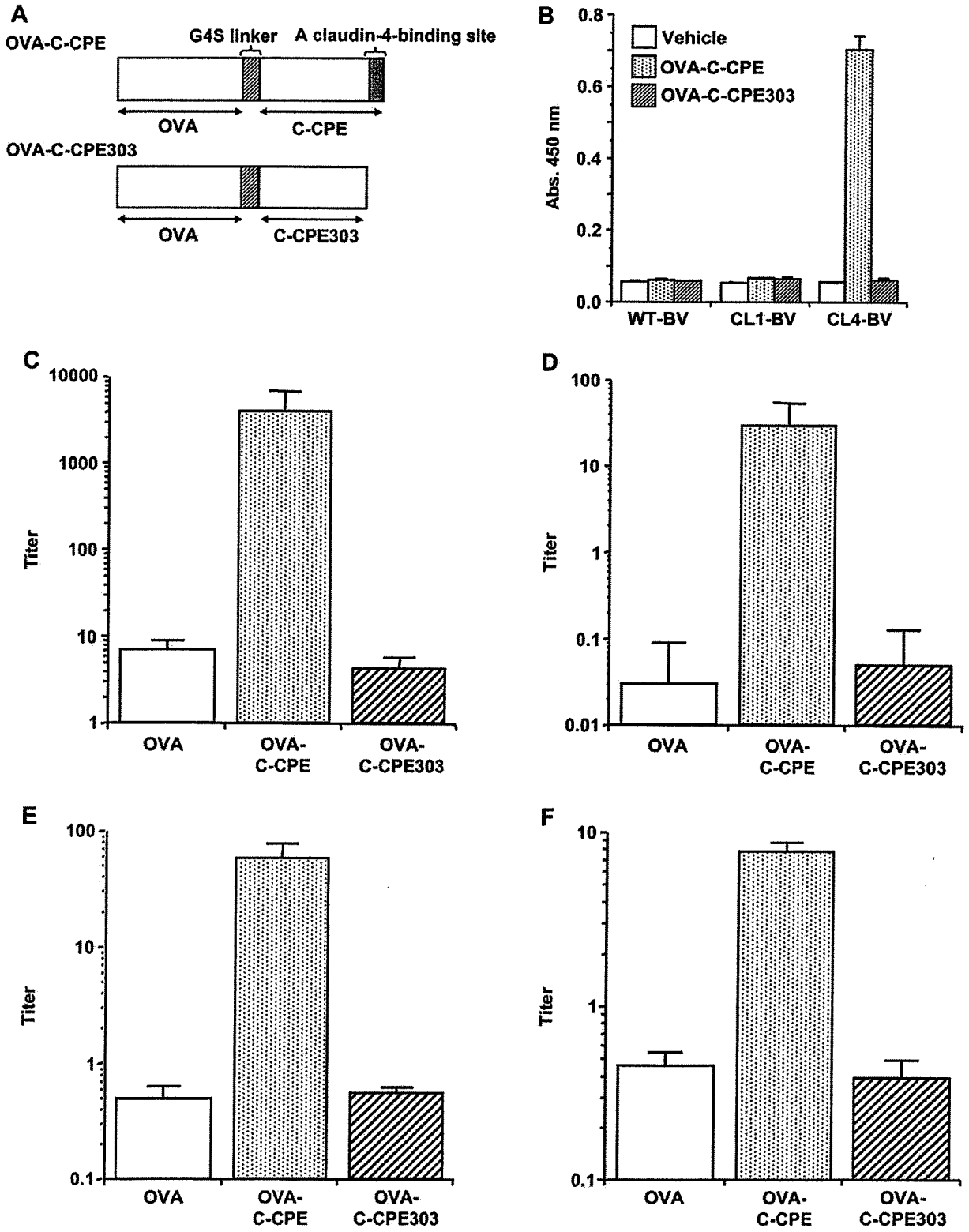

Fig. 4. Involvement of claudin-4 in the immune responses to OVA-C-CPE. A) Schematic illustration of OVA-C-CPE mutant. The C-terminal 16 amino acid-deleted C-CPE mutant (C-CPE303) did not bind to claudin-4 [29]. To clarify the involvement of claudin-4 in the immune response initiated by OVA-C-CPE, OVA was fused with C-CPE303, resulting in OVA-C-CPE303. B) Interaction of OVA-C-CPE303 with claudin-4. Binding of OVA-C-CPE303 to claudin-4 was investigated by ELISA with wild-type BV (WT-BV), claudin-1 or -4-displaying BV (CL1-BV, CL4-BV). C) Immune responses by OVA-C-CPE303. Mice were nasally immunized with OVA, OVA-C-CPE or OVA-C-CPE303 (5 μg OVA) once a week for 3 weeks. Seven days after the last immunization, the levels of serum IgG (C), nasal IgA (D), vaginal IgA (E) and fecal IgA (F) were measured by ELISA. Data are means ± SD ($n = 4$). Data are representative of three independent experiments.

Please cite this article in press as: Kakutani H, et al., Mucosal vaccination using claudin-4-targeting, Biomaterials (2010), doi:10.1016/j.biomaterials.2010.03.047

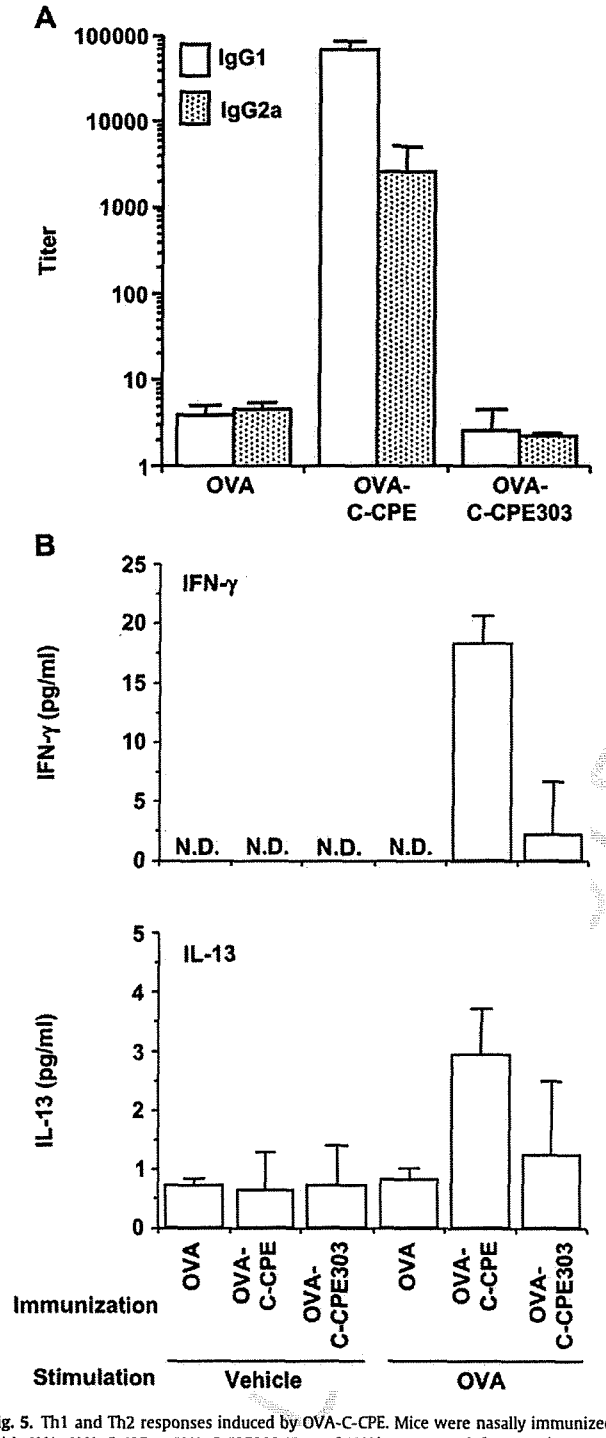

Fig. 5. Th1 and Th2 responses induced by OVA-C-CPE. Mice were nasally immunized with OVA, OVA-C-CPE or OVA-C-CPE303 (5 μg of OVA) once a week for 3 weeks. Seven days after the last immunization, serum and splenocytes were collected. Serum IgG subclass (IgG1 and IgG2a) was determined by ELISA (A). The splenocytes isolated from the immunized mice were stimulated with vehicle or OVA (1 mg/ml) for 24 h, and the cytokines (IFN-γ and IL-13) in the conditioned medium were measured by ELISA (B). Data are means ± SD ($n = 4$). N.D., not detected.

Th2 responses in IgG production and cytokines production were not observed in mice nasally immunized with OVA-C-CPE303 (Fig. 5A and B). These data indicate that claudin-4-targeting may be a potent method for mucosal vaccination.

3.5. Anti-tumor immune response induced by the claudin-4-targeting vaccine

To evaluate the immune responses induced by nasal vaccination with OVA-C-CPE, we performed an in vivo anti-tumor assay with EG7 thymoma cells, which are syngeneic tumor cells derived from OVA cDNA-transfected EL4 thymoma cells [33]. C57BL/6 mice were immunized with vehicle, OVA, a mixture of OVA and C-CPE, or OVA-C-CPE once a week for 3 weeks. Seven days after the last immunization, mice were challenged with EG7 thymoma cells. Tumor growth was monitored by calculating the average tumor volume. As shown in Fig. 6A, tumor growth was significantly suppressed in mice immunized with OVA-C-CPE, whereas the tumor growth was not suppressed in mice immunized with OVA or a mixture of OVA and C-CPE. Immunization with OVA-C-CPE303, in which the claudin-4-binding region was deleted, did not induce a protective immune response against tumor challenge. Immunization with OVA or OVA-C-CPE303 did not stimulate Th1- and Th2-immune responses including IgG1, IgG2a, IFN-γ and IL-13 production; whereas immunization with OVA-C-CPE stimulated these immune responses (Fig. 6B and C). These data indicate that nasal immunization with a claudin-4-targeting vaccine may be useful for cancer therapy.

4. Discussion

Recent progress in vaccine development has provided new insight into vaccine therapies for not only infectious diseases but also cancer, Alzheimer disease and Parkinson disease [3,34]. Mucosal vaccination, such as oral, nasal and pulmonary immunization, has greater therapeutic potential and increased patient comfort as compared to parenteral vaccination. The nasal cavity is the most promising site since it has low enzymatic activity and highly available immunoreactive sites; however, immunoresponses are not stimulated by intranasal administration of antigens [15,35–37]. Efficient delivery of antigens to NALT is critical for the development of nasal vaccines. In the present study, we found that intranasal immunization with antigen fused with a claudin-4-binder, C-CPE, stimulated humoral and mucosal immune responses and that these immune responses did not occur when the claudin-4-binding domain was deleted.

How does OVA-C-CPE activate immune responses? Claudin plays a pivotal role in the TJ-barrier in epithelium [38]. We previously found that C-CPE modulates the claudin-4 barrier and enhances mucosal absorption of dextran [30]. Activation of immune responses by OVA-C-CPE may be caused by modulation of the epithelial barrier in NALT, resulting in the uptake of OVA-C-CPE or its degradable product into NALT. OVA-C-CPE modulated the epithelial barrier in a human intestinal model of Caco-2 monolayer cells (data not shown). C-CPE enhanced jejunal absorption of dextran with a molecular mass of 4–20 kDa, and the integrity of the epithelial barrier in nasal mucosa was similar to that in jejunal mucosa [30,39]. OVA-C-CPE, which has a molecular mass of 62 kDa, may be poorly absorbed by nasal tissue. When OVA-C-CPE is degraded into fragments with a molecular mass of less than 20 kDa, the OVA fragment might be absorbed across nasal epithelium. A mixture of OVA and C-CPE did not induce an immune response, and deletion of the claudin-4-binding region in OVA-C-CPE attenuated the immune responses caused by nasal immunization with OVA-C-CPE. These findings indicate that targeting to claudin-4 rather than modulating the claudin-4 barrier by C-CPE is involved in the immune response to nasal vaccinations of OVA-C-CPE.

What cells are taken up OVA-C-CPE? NALT is covered by a unique epithelial layer known as FAE. Lymphocytes, T cells, B cells and APCs underlie the FAE. Antigen presentation to the

Please cite this article in press as: Kakutani H, et al., Mucosal vaccination using claudin-4-targeting, Biomaterials (2010), doi:10.1016/j.biomaterials.2010.03.047

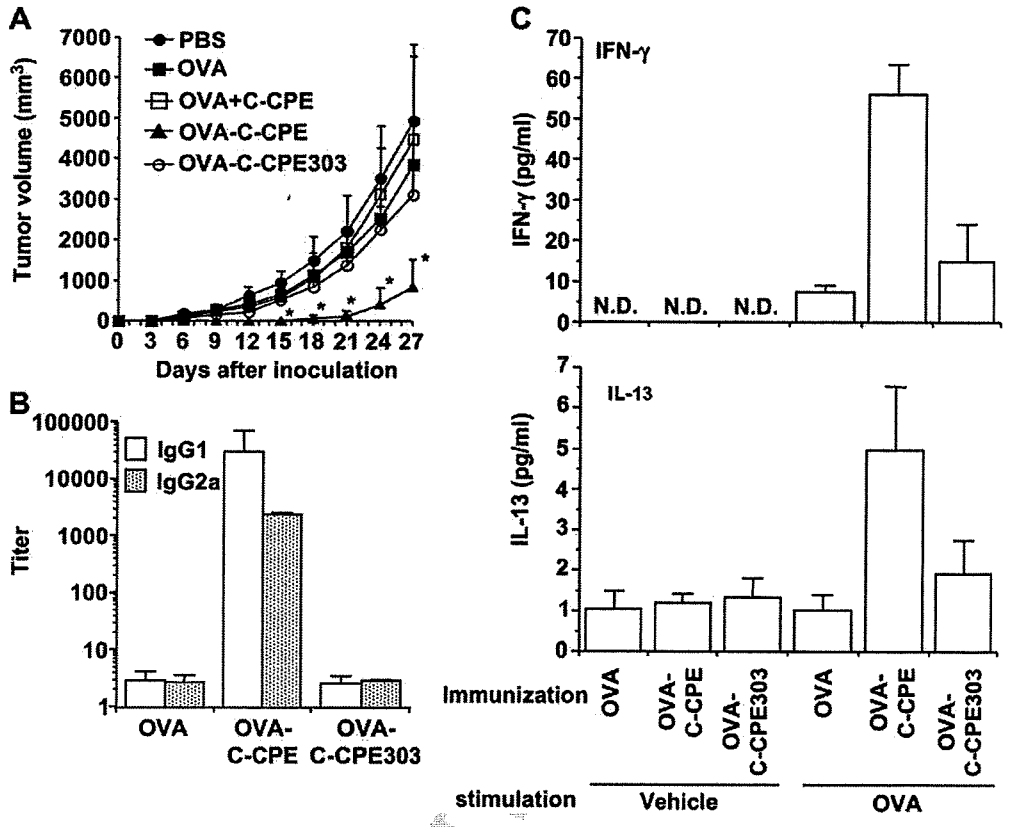

Fig. 6. Anti-tumor activity induced by immunization with OVA-C-CPE in an EG7 cancer model. A) Protective immune response against tumor challenge. C57BL/6 mice were nasally immunized with vehicle, OVA, a mixture of OVA and C-CPE, OVA-C-CPE, or OVA-C-CPE303 (5 μg of OVA) once a week for 3 weeks. Seven days after the last immunization, the mice were injected s.c. on the right back with 1×10^6 EG7 cells. The tumor volumes were calculated as described in the Materials and methods. Data are means ± SD ($n = 4$). The results are representative of two independent experiments. *Significantly different from the vehicle-immunized group ($P < 0.05$). B, C) Immune responses in the cancer model. Mice were nasally immunized with vehicle, OVA, OVA-C-CPE, or OVA-C-CPE303 (5 μg of OVA) once a week for 3 weeks. Seven days after the last immunization, the serum and splenocytes were recovered. Serum IgG subclass (IgG1 and IgG2a) was determined by ELISA (B). The splenocytes were stimulated with vehicle or OVA (1 mg/ml) for 24 h, and the cytokines (IFN-γ and IL-13) in the conditioned medium were measured by ELISA (C). Data are means ± SD ($n = 4$). N.D., not detected. The results are representative of two independent experiments.

immunocompetent cells by FAE is a trigger of mucosal immune responses [40,41]. Claudin-4 is expressed in the FAE of MALT [22]. Claudin-4 contains clathrin-sorting signal sequences in its C-terminal intracellular region [42,43]; thus, it may be taken up by clathrin-mediated endocytosis. Indeed, Matsuda et al. (2004) showed the endocytosis of claudins during the remodeling of TJs [44], and a C-CPE-fused molecule was intracellularly taken up [27]. OVA-C-CPE may be taken up into FAE followed by the presentation of antigens to the underlying immunocompetent cells. The FAE is enriched with specialized antigen-sampling epithelial cells known as M cells. M cells form an apparent pocket at the basal membrane site, and this pocket contains T cells, B cells, macrophages and dendritic cells. M cells deliver samples of foreign material by active transepithelial vesicular transport from the lumen directly to intraepithelial lymphoid cells and to subepithelial organized lymphoid tissue [6,16,40]. An antigen delivery system to M cells has been developed, and ligands for M cells, including a lectin, a peptide or a specific antibody, have been used for mucosal vaccination [45–48]. It has not been determined if claudin-4 is expressed in M cells and if OVA-C-CPE is taken up into M cells. Further investigation to clarify the mode of action of the claudin-4-targeting vaccine is needed.

Safety is essential for clinical application of the claudin-4-targeting vaccine. Histological injury was not detected after the administration of OVA-C-CPE. C-CPE is the receptor-binding domain of CPE without the cytotoxic domain [24,49]. Claudin functions as an epithelial barrier between the inside and the outside of the body, and modulation of the claudin-4 barrier by the claudin-4 binder may cause side effects due to the non-specific influx of xenobiotics through the loosened epithelial barrier. The claudin family contains more than 20 members, and the claudin expression and barrier-function differ among tissues [38,50]. Expression profiles of claudin in the mucosal epithelium also differ among the sites of epithelium [51,52]. To reduce the risk of solute influx, further investigation of the difference in claudin expression between MALT and the other sites is important. Preparation of a claudin binder with less modulation of the epithelial barrier is also needed.

In rodents, NALT is found on both sides of the nasopharyngeal duct dorsal to the cartilaginous soft palate. Humans do not have NALT, except at an early age [53]; but, they possess oropharyngeal lymphoid tissues, including unpaired nasopharyngeal tonsils (adenoids) and bilateral tubular palatine, and lingual tonsils (Waldeyer's ring), which seem to correspond functionally to NALT [7,54]. The expression of claudin-4 in the human MALT, such as the tonsils and adenoids, should be investigated for the development of oral mucosal vaccine.

5. Conclusions

In the present study, we prepared C-CPE-fused OVA, and we found that the intranasal administration of the fusion protein increased not

Please cite this article in press as: Kakutani H, et al., Mucosal vaccination using claudin-4-targeting, Biomaterials (2010), doi:10.1016/j.biomaterials.2010.03.047

only nasal IgA levels but also OVA-specific serum IgG, vaginal IgA and fecal IgA levels. Moreover, deletion of the claudin-4-binding region in the fusion protein caused the loss of immunomodulating activities. The claudin-4-targeting antigen immunization activated both Th1 and Th2 responses and showed anti-tumor activity in mice inoculated with OVA-expressing thymoma cells. This is the first report to indicate that claudin-4-targeting may be a promising strategy for the development of mucosal vaccines.

Acknowledgements

We thank Drs Y. Horiguchi, S. Nakagawa (Osaka University), M. Furuse (Kobe University) and J. Kunisawa (The University of Tokyo) for providing C-CPE cDNA, OVA cDNA, claudin cDNA and useful comments, respectively. We also thank the all members of our laboratory for their useful comments and discussion. This work was supported by a Grant-in-Aid for Scientific Research from the Ministry of Education, Culture, Sports, Science and Technology, Japan (21689006), by a Health and Labor Sciences Research Grants from the Ministry of Health, Labor and Welfare of Japan, by Takeda Science Foundation, by a Suzuken Memorial Foundation, by a grant from Kansai Biomedical Cluster project in Saito, which is promoted by the Knowledge Cluster Initiative of the Ministry of Education, Culture, Sports, Science and Technology, Japan, by a Research Grant for Promoting Technological Seeds from Japan Science and Technology Agency and the Japan Health Sciences Foundation.

References

[1] Boyaka PN, Marinaro M, Vancott JL, Takahashi I, Fujihashi K, Yamamoto M, et al. Strategies for mucosal vaccine development. Am J Trop Med Hyg 1999;60:35–45.
[2] Cardenas-Freytag L, Cheng E, Mirza A. New approaches to mucosal immunization. Adv Exp Med Biol 1999;473:319–37.
[3] Michels KB, zur Hausen H. HPV vaccine for all. Lancet 2009;374:268–70.
[4] Neutra MR, Kozlowski PA. Mucosal vaccines: the promise and the challenge. Nat Rev Immunol 2006;6:148–58.
[5] Ryan EJ, Daly LM, Mills KH. Immunomodulators and delivery systems for vaccination by mucosal routes. Trends Biotechnol 2001;19:293–304.
[6] Yuki Y, Kiyono H. New generation of mucosal adjuvants for the induction of protective immunity. Rev Med Virol 2003;13:293–310.
[7] Kiyono H, Fukuyama S. NALT-versus Peyer's-patch-mediated mucosal immunity. Nat Rev Immunol 2004;4:699–710.
[8] Kunisawa J, Fukuyama S, Kiyono H. Mucosa-associated lymphoid tissues in the aerodigestive tract: their shared and divergent traits and their importance to the orchestration of the mucosal immune system. Curr Mol Med 2005;5:557–72.
[9] Kunisawa J, Nochi T, Kiyono H. Immunological commonalities and distinctions between airway and digestive immunity. Trends Immunol 2008;29:505–13.
[10] Imaoka K, Miller CJ, Kubota M, McChesney MB, Lohman B, Yamamoto M, et al. Nasal immunization of nonhuman primates with simian immunodeficiency virus p55gag and cholera toxin adjuvant induces Th1/Th2 help for virus-specific immune responses in reproductive tissues. J Immunol 1998;161:5952–8.
[11] Rudin A, Riise GC, Holmgren J. Antibody responses in the lower respiratory tract and male urogenital tract in humans after nasal and oral vaccination with cholera toxin B subunit. Infect Immun 1999;67:2884–90.
[12] Staats HF, Montgomery SP, Palker TJ. Intranasal immunization is superior to vaginal, gastric, or rectal immunization for the induction of systemic and mucosal anti-HIV antibody responses. AIDS Res Hum Retroviruses 1997;13:945–52.
[13] Gallichan WS, Rosenthal KL. Long-term immunity and protection against herpes simplex virus type 2 in the murine female genital tract after mucosal but not systemic immunization. J Infect Dis 1998;177:1155–61.
[14] Kozlowski PA, Williams SB, Lynch RM, Flanigan TP, Patterson RR, Cu-Uvin S, et al. Differential induction of mucosal and systemic antibody responses in women after nasal, rectal, or vaginal immunization: influence of the menstrual cycle. J Immunol 2002;169:566–74.
[15] Zinkernagel RM. Localization dose and time of antigens determine immune reactivity. Semin Immunol 2000;12:163–71.
[16] Neutra MR, Frey A, Kraehenbuhl JP. Epithelial M cells: gateways for mucosal infection and immunization. Cell 1996;86:345–8.
[17] Owen RL. Sequential uptake of horseradish peroxidase by lymphoid follicle epithelium of Peyer's patches in the normal unobstructed mouse intestine: an ultrastructural study. Gastroenterology 1977;72:440–51.
[18] Owen RL, Piazza AJ, Ermak TH. Ultrastructural and cytoarchitectural features of lymphoreticular organs in the colon and rectum of adult BALB/c mice. Am J Anat 1991;190:10–8.
[19] Scheneeberger EE, Lynch RD. Structure, function, and regulation of cellular tight junctions. Am J Physiol 1992;262:L647–61.
[20] Tsukita S, Furuse M, Itoh M. Multifunctional strands in tight junctions. Nat Rev Mol Cell Biol 2001;2:285–93.
[21] Mitic LL, Van Itallie CM, Anderson JM. Molecular physiology and pathophysiology of tight junctions I. Tight junction structure and function: lessons from mutant animals and proteins. Am J Physiol 2000;279:G250–4.
[22] Tamagawa H, Takahashi I, Furuse M, Yoshitake-Kitano Y, Tsukita S, Ito T, et al. Characteristics of claudin expression in follicle-associated epithelium of Peyer's patches: preferential localization of claudin-4 at the apex of the dome region. Lab Invest 2003;83:1045–53.
[23] McClane BA, Chakrabarti G. New insights into the cytotoxic mechanisms of *Clostridium perfringens* enterotoxin. Anaerobe 2004;10:107–14.
[24] Katahira J, Inoue N, Horiguchi Y, Matsuda M, Sugimoto N. Molecular cloning and functional characterization of the receptor for *Clostridium perfringens* enterotoxin. J Cell Biol 1997;136:1239–47.
[25] Sonoda N, Furuse M, Sasaki H, Yonemura S, Katahira J, Horiguchi Y, et al. *Clostridium perfringens* enterotoxin fragment removes specific claudins from tight junction strands: evidence for direct involvement of claudins in tight junction barrier. J Cell Biol 1999;147:195–204.
[26] Van Itallie CM, Betts L, Smedley 3rd JG, McClane BA, Anderson JM. Structure of the claudin-binding domain of *Clostridium perfringens* enterotoxin. J Biol Chem 2008;283:268–74.
[27] Ebihara C, Kondoh M, Hasuike N, Harada M, Mizuguchi H, Horiguchi Y, et al. Preparation of a claudin-targeting molecule using a C-terminal fragment of *Clostridium perfringens* enterotoxin. J Pharmacol Exp Ther 2006;316:255–60.
[28] Saeki R, Kondoh M, Kakutani H, Tsunoda S, Mochizuki Y, Hamakubo T, et al. A novel tumor-targeted therapy using a claudin-4-targeting molecule. Mol Pharmacol 2009;76:918–26.
[29] Takahashi A, Kondoh M, Masuyama A, Fujii M, Mizuguchi H, Horiguchi Y, et al. Role of C-terminal regions of the C-terminal fragment of *Clostridium perfringens* enterotoxin in its interaction with claudin-4. J Control Release 2005;108:56–62.
[30] Kondoh M, Masuyama A, Takahashi A, Asano N, Mizuguchi H, Koizumi N, et al. A novel strategy for the enhancement of drug absorption using a claudin modulator. Mol Pharmacol 2005;67:749–56.
[31] Yamamoto S, Kiyono H, Yamamoto M, Imaoka K, Fujihashi K, Van Ginkel FW, et al. A nontoxic mutant of cholera toxin elicits Th2-type responses for enhanced mucosal immunity. Proc Natl Acad Sci USA 1997;94:5267–72.
[32] Yanagita M, Hiroi T, Kitagaki N, Hamada S, Ito HO, Shimauchi H, et al. Nasopharyngeal-associated lymphoreticular tissue (NALT) immunity: fimbriae-specific Th1 and Th2 cell-regulated IgA responses for the inhibition of bacterial attachment to epithelial cells and subsequent inflammatory cytokine production. J Immunol 1999;162:3559–65.
[33] Moore MW, Carbone FR, Bevan MJ. Introduction of soluble protein into the class I pathway of antigen processing and presentation. Cell 1988;54:777–85.
[34] Boche D, Nicoll JA, Weller RO. Immunotherapy for Alzheimer's disease and other dementias. Clin Neuropharmacol 2006;29:22–7.
[35] Dahl R, Mygind N. Anatomy, physiology and function of the nasal cavities in health and disease. Adv Drug Deliv Rev 1998;29:3–12.
[36] Ugwoke MI, Agu RU, Verbeke N, Kinget R. Nasal mucoadhesive drug delivery: background, applications, trends and future perspectives. Adv Drug Deliv Rev 2005;57:1640–65.
[37] Ugwoke MI, Verbeke N, Kinget R. The biopharmaceutical aspects of nasal mucoadhesive drug delivery. J Pharm Pharmacol 2001;53:3–21.
[38] Furuse M, Tsukita S. Claudins in occluding junctions of humans and flies. Trends Cell Biol 2006;16:181–8.
[39] Rojanasakul Y, Wang LY, Bhat M, Glover DD, Malanga CJ, Ma JK. The transport barrier of epithelia: a comparative study on membrane permeability and charge selectivity in the rabbit. Pharm Res. 1992;9:1029–34.
[40] Kraehenbuhl JP, Neutra MR. Molecular and cellular basis of immune protection of mucosal surfaces. Physiol Rev 1992;72:853–79.
[41] Neutra MR, Mantis NJ, Kraehenbuhl JP. Collaboration of epithelial cells with organized mucosal lymphoid tissues. Nat Immunol 2001;2:1004–9.
[42] Bonifacino JS, Traub LM. Signals for sorting of transmembrane proteins to endosomes and lysosomes. Annu Rev Biochem 2003;72:395–447.
[43] Ivanov AI, Nusrat A, Parkos CA. Endocytosis of epithelial apical junctional proteins by a clathrin-mediated pathway into a unique storage compartment. Mol Biol Cell 2004;15:176–88.
[44] Matsuda M, Kubo A, Furuse M, Tsukita S. A peculiar internalization of claudins, tight junction-specific adhesion molecules, during the intercellular movement of epithelial cells. J Cell Sci 2004;117:1247–57.
[45] Higgins LM, Lambkin I, Donnelly G, Byrne D, Wilson C, Dee J, et al. In vivo phage display to identify M cell-targeting ligands. Pharm Res. 2004;21:695–705.

Please cite this article in press as: Kakutani H, et al., Mucosal vaccination using claudin-4-targeting, Biomaterials (2010), doi:10.1016/j.biomaterials.2010.03.047

[46] Manocha M, Pal PC, Chitralekha KT, Thomas BE, Tripathi V, Gupta SD, et al. Enhanced mucosal and systemic immune response with intranasal immunization of mice with HIV peptides entrapped in PLG microparticles in combination with Ulex Europaeus-I lectin as M cell target. Vaccine 2005;23:5599–617.

[47] Nochi T, Yuki Y, Matsumura A, Mejima M, Terahara K, Kim DY, et al. A novel M cell-specific carbohydrate-targeted mucosal vaccine effectively induces antigen-specific immune responses. J Exp Med 2007;204:2789–96. .

[48] Wang X, Kochetkova I, Haddad A, Hoyt T, Hone DM, Pascual DW. Transgene vaccination using Ulex europaeus agglutinin I (UEA-1) for targeted mucosal immunization against HIV-1 envelope. Vaccine 2005;23:3836–42.

[49] Hanna PC, Wieckowski EU, Mietzner TA, McClane BA. Mapping of functional regions of *Clostridium perfringens* type A enterotoxin. Infect Immun 1992;60:2110–4.

[50] Morita K, Furuse M, Fujimoto K, Tsukita S. Claudin multigene family encoding four-transmembrane domain protein components of tight junction strands. Proc Natl Acad Sci USA 1999;96:511–6.

[51] Chiba H, Osanai M, Murata M, Kojima T, Sawada N. Transmembrane proteins of tight junctions. Biochim Biophys Acta 2008;1778:588–600.

[52] Rahner C, Mitic LL, Anderson JM. Heterogeneity in expression and subcellular localization of claudins 2, 3, 4, and 5 in the rat liver, pancreas, and gut. Gastroenterology 2001;120:411–22.

[53] Debertin AS, Tschernig T, Tonjes H, Kleemann WJ, Troger HD, Pabst R. Nasal-associated lymphoid tissue (NALT): frequency and localization in young children. Clin Exp Immunol 2003;134:503–7.

[54] Koornstra PJ, de Jong FI, Vlek LF, Marres EH, van Breda Vriesman PJ. The Waldeyer ring equivalent in the rat. A model for analysis of oronasopharyngeal immune responses. Acta Otolaryngol 1991;111:591–9.

Please cite this article in press as: Kakutani H, et al., Mucosal vaccination using claudin-4-targeting, Biomaterials (2010), doi:10.1016/j.biomaterials.2010.03.047

Journal of Electron Microscopy Advance Access published November 11, 2009

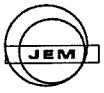

Journal of Electron Microscopy: 1–10 (2009)
doi: 10.1093/jmicro/dfp056

Physical: Full-length—Experimental

Morphological study of acoustic liposomes using transmission electron microscopy

Tetsuya Kodama[1,*], Noriko Tomita[1,5], Sachiko Horie[1], Nicolas Sax[1], Hiroko Iwasaki[1], Ryo Suzuki[2], Kazuo Maruyama[2], Shiro Mori[3] and Fukumoto Manabu[4]

[1]Graduate School of Biomedical Engineering, Tohoku University, 2-1 Seiryo, Aoba, Sendai, 980-8575, Japan, [2]Department of Biopharmaceutics, School of Pharmaceutical Sciences, Teikyo University, 1091-1 Suwarashi, Sagamiko, Sagamihra, Kanagawa, 229-0195, Japan, [3]Department of Oral Health Science, Tohoku University Hospital, 1-1 Seiryo, Aoba, Sendai, 980-8574, Japan and [4]Institute of Development, Aging and Cancer, Tohoku University, 4-1 Seiryo, Aoba, Sendai, 980-8575, Japan
[5]Present address: Institute of Fluid Science, Tohoku University, 2-1-1 Katahira, Aoba, Sendai, 980-8577, Japan
*To whom correspondence should be addressed. E-mail: kodama@bme.tohoku.ac.jp

Abstract Sonoporation is achieved by ultrasound-mediated destruction of ultrasound contrast agents (UCA) microbubbles. For this, UCAs must be tissue specific and have good echogenicity and also function as drug carriers. Previous studies have developed acoustic liposomes (ALs), liposomes that encapsulate phosphate buffer solution and perfluoropropane (C_3F_8) gas and function as both UCAs and drug carriers. Few studies have examined the co-existence of gas and liquid in ALs. This study aims to elucidate AL structure using TEM. The size, zeta potential and structure of ALs were compared with those of two other UCAs, human albumin shell bubbles (ABs; Optison) and lipid bubbles (LBs). ABs and LBs encapsulate the C_3F_8 gas. Particle size was measured by dynamic light scattering. The zeta potential was determined by the Smoluchowski equation. UCA structure was investigated by TEM. ALs were ~200 nm in size, smaller than LBs and ABs. ALs and LBs had almost neutral zeta potentials whereas AB values were strongly negative. The negative or double staining TEM images revealed that ~20% of ALs contained both liquid and gas, while ~80% contained liquid alone (i.e. nonacoustic). Negative staining AB images indicated electron beam scattering near the shell surface, and albumin was detected in filament form. These findings suggest that AL is capable of carrying drugs and high-molecular-weight, low-solubility gases.

Keywords nanobubbles, drug delivery system, sonoporation, ultrasound contrast agent, cavitation

Received 25 June 2009, accepted 5 October 2009

Introduction

Ultrasound contrast agents (UCAs) are nano/microbubbles that contain air or a high-molecular-weight, low water-solubility gas (e.g. C_3F_8, C_4F_{10} and SF_6) encapsulated in a lipid or albumin shell [1–6]. The diameters of UCAs vary from 100 nm to 10 μm and their behavior primarily depends on the ultrasound characteristics. The behavior of UCAs is described by an equation of motion that consists of external force, viscosity and stiffness terms [7]. When the external force is small, i.e. ultrasound pressure is small, UCAs undergo small volumetric oscillation (linear). With increasing ultrasound pressures, the amplitude of volumetric oscillation increases and

oscillation becomes aperiodic (nonlinear), resulting in destruction of UCAs [1,8].

Drug delivery via sonoporation using ultrasound and UCAs is a technique used for diagnosis and treatment [1,8] and is based on bubble destruction modes. During sonoporation, primary UCAs and subsequent bubble cavitation generated by the collapse of the UCAs induce mechanical forces such as liquid jets and shock waves [8]. These forces interact with the surrounding cells, resulting in the permeation of exogenous molecules into cells [1,8]. Sonoporation is a noninvasive, nonimmunogenic and tissue-specific procedure that has been used to treat cancer and many other diseases [1,3,9]. However, the efficiency of molecular delivery is relatively low; therefore, it has not been recognized as a clinically valuable approach. One strategy towards improving the efficiency of molecular delivery is to develop UCAs that are tissue-specific and that can function as drug carriers. Suzuki *et al.* [9] developed a novel form of liposome containing the C_3F_8 gas and phosphate buffer solution and demonstrated that it functions as an acoustic liposome (AL) applicable to a nonvirus molecular delivery system [5,6]. The liposome surface was covered with polyethyleneglycol (PEG); therefore, it was assumed that this molecule would not be incorporated by the reticuloendothelial system, thereby allowing a longer retention in the blood [10]. In addition, the tumor-targeting potential and drug-carrying capability are significantly improved by conjugating PEG with ligands specific for the target tissue and by producing bubbles with diameters of <100 nm, which allows for enhanced permeability and retention (EPR) effects [11,12]. These studies concluded that the liposome would be acoustic due to the differences between ultrasound backscatter intensities in the presence/absence of ultrasound. However, the coexistence of gas and liquid in the liposome has not been examined, neither have its size and structure been discussed.

The present study investigated the size, zeta potential and structure of ALs and compared these values with those of two other types of UCAs: a single human albumin shell (ABs; Optison) and lipid bubbles (LBs). Both UCAs encapsulated the C_3F_8 gas, which was identical to the liposome gas. Transmission electron microscopy (TEM) was used to assess the structure of UCAs, and the TEM images were obtained using either negative or double staining. The TEM findings will be used as parameters to evaluate biodistribution, safety and efficacy of micro/nanoparticulate systems.

Methods

Nano/microbubble preparation

Three types of UCA—ABs ($5.0–8.0 \times 10^8$ bubbles mL^{-1}; Optison™, Amersham Health Plc, Oslo, Norway), LBs and ALs—were used. LBs were created in an aqueous dispersion of 2 mg mL^{-1} 1,2-distearoyl-sn-glycero-phosphatidylcholine (DSPC) (Avanti Polar Lipids, Alabaster, AL, USA) and 1 mg mL^{-1} polyethylene glycol (PEG) distearate (Sigma-Aldrich) using a 20 kHz stick sonicator (130 W, Vibra Cell, Sonics & Materials Inc., Danbury, CT, USA) at 50% amplifying strength for 1 min, in the presence of C_3F_8 gas in a sterilized 7 mL Bijou vial [8,13,14]. The vial cap has two openings that serve as a gas inlet and outlet. During sonication, the C_3F_8 gas was kept under the condition of inflow and outflow through the openings. The LB concentration was 3.4×10^8 bubbles mL^{-1} [13]. ALs were prepared by modifying the protocol of Suzuki *et al.* [9]. First, DSPC (NOF Co., Tokyo, Japan) and 1,2-distearoyl-sn-glycero-3-phosphatidyl-ethanolamine-methoxy-polyethyleneglycol (DSPE-PEG2000-OMe) (NOF Co.) (94:6 [mol/mol]) were dissolved in 10 mL of 9:1 (v/v) chloroform/methanol. Next, 5 mL of phosphate-buffered saline (PBS) without Mg^{2+} and Ca^{2+} (pH 7.2 at room temperature, Sigma) was added to the solution. The solution was then sonicated using a 20 kHz stick sonicator (Sonics & Materials). Liposomes were obtained by reverse phase evaporation at 65°C. The organic solvent was completely removed, and the size of the liposomes was adjusted to <100 nm using extruding equipment (Northern Lipids Inc., Vancouver, BC, Canada) with three sizing filters (pore sizes: 100, 200 and 600 nm) (Nuclepore Track-Etch Membrane, Whatman plc, UK). The resulting liposomes were passed through a 0.45 μm pore size filter (MILLEX HV filter unit, Durapore polyvinylidine-difluoride (PVDF) membrane, Millipore Corporation, MA, USA) for sterilization. Lipid concentration was measured using the Phospholipid *C*-test Wako (Wako Pure Chemical Industries, Ltd, Osaka, Japan). To produce AL, a

liposome suspension of 1 mL (lipid concentration: 1 mg mL^{-1}) was sonicated using a bath sonicator (42 kHz, 100 W; Bransonic 2510J-DTH, Branson Ultrasounics Co., Danbury, CT, USA) and a 20 kHz stick sonicator (130 W, Sonics & Materials, Inc.) at 50% amplifying strength for 1 min, in the presence of C_3F_8 in a sterilized 7 mL Bijou vial, as described above.

Dark field microscopy

Immediately after sonication, 20 μL drops of either AL or LB were put on a glass cover and were observed under an inverted microscope (IX81, Olympus, Tokyo, Japan) equipped with an illuminator (Darlkite Illuminator, Micro Video Instruments, Avon, MA , USA).

Echogenicity measurement

The air inside the 5 mL vials containing 1 mL of liposome suspension (lipid concentration: 1 mg mL^{-1}) sealed with a rubber cap together with an aluminium jacket was replaced with 12 mL of air or C_3F_8 gas and supercharged with another 12 mL of each gas. The suspension in the vial was sonicated in a bath sonicator (Branson Ultrasounics) for 2 min. The suspension was transferred to a 7 mL Bijou vial and further sonicated by a 20 kHz sonicator (Sonics & Materials) at 50% amplifying strength for 1 min while 5 mL of each gas was injected at a rate of 300 mL h^{-1} using a syringe pump (model KDS 100, KD Scientific, Holliston, MA, USA). Four milliliters of a 40-fold dilution with PBS were added to a well of a 6-well plate and the B-mode image was acquired with a high-frequency ultrasound imaging system with a center frequency of 55 MHz (VEVO 770, Visualsonics Inc., Toronto, Canada). The grayscale histogram of a selected ROI was measured using the implemented software of the US imaging system. The ROI circle was set to 1.00 mm^2, 1 mm above the bottom of the well.

Size and zeta potential

The size and zeta potentials of the bubbles were measured using a zeta potential & particle size analyzer (zeta potential range: −200 to +200 mV, particle size/distribution range: 0.6 nm to 7 μm, laser source: laser diode (660 nm), ELSZ-2, Otsuka Electronics, Osaka, Japan). The size was measured using the dynamic light scattering. The zeta potential was automatically calculated on the basis of the electrophoretic mobility using the Smoluchowski equation: $\zeta = 4\pi\eta u/\varepsilon$, where ζ is the zeta potential, u is the electrophoretic mobility and η and ε are the viscosity and dielectric constant of the solvent, respectively. The Smoluchowski equation is applicable to a solid surface on which a surface-charge layer exits and electrolyte ions do not penetrate through the surface, i.e. hard particles [15]. In the present study, the three types of bubbles were assumed to be hard particles. The bubble solutions were diluted in PBS to $\sim 10^7$ bubbles mL^{-1} at room temperature (21–23°C). The average values of the sizes and zeta potentials were calculated using four to nine independent measurements on each sample.

TEM

Either negative or double staining was used for AL. Negative staining was used for LB and AB. The stained samples were examined with a JEM-2000EX operated at 100 kV (JEOL Datum, Tokyo, Japan) at the Hanaichi UltraStructure Research Institute, Aichi, Japan; or with a H-7600 operated at 80 kV (Hitachi Tokyo, Japan) at Tohoku University, Sendai, Japan. For the negative staining, a 400-mesh grid (EM fine-grid F-400, Nisshin EM Co., Tokyo, Japan) with a carbon support film (10–20 nm in thickness) was used, and was given a hydrophilic treatment. Samples were stained at either room temperature or at 80°C. For the former case, a drop of sample solution, distilled water and phosphotungstic acid (Merck, Tokyo, Japan) were put on a parafilm (Pechiney Plastic Packaging Co., Menasha, WI, USA). The grid was put into the sample drop (30 s), then in a distilled water drop for washing (10 s) and finally in a phosphotungstic acid drop for staining (10 s). Any excess solution was removed with filter paper. For the latter case, a parafilm was floated on water heated at 80 °C, and the procedure outlined above was then followed. For the double staining, an AL solution generated in the presence of C_3F_8 in a sterilized 7 mL vial was immediately added to 1 mL of 2% agarose (Cambrex Bio Science Rockland, Inc., Rockland, USA) to obtain a stable solution that did not release gas. Then, the AL solution was mixed with the same amount of

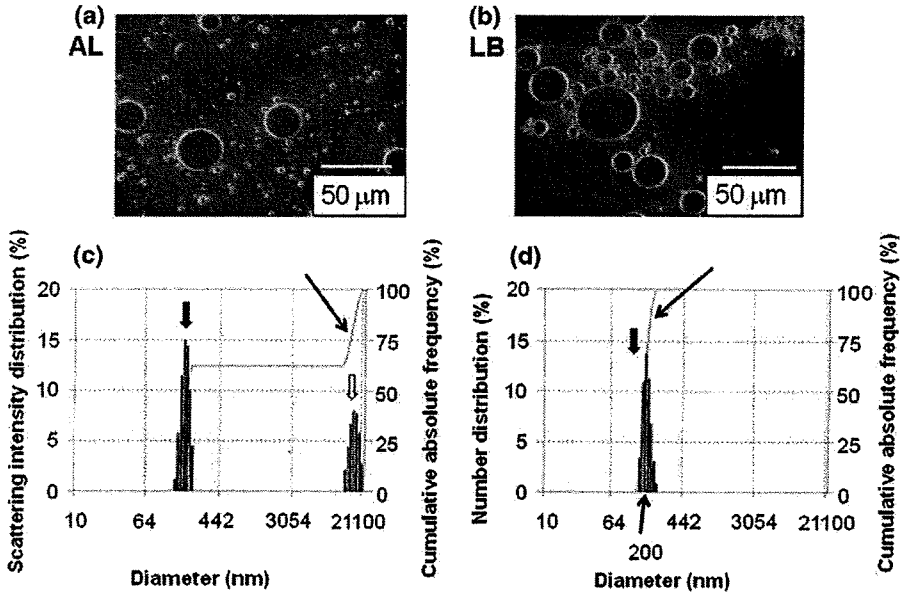

Fig. 1. Dark field images of ALs and LBs and size distribution of ALs. (a) AL dark field image. (b) LB dark field image. (c) Scattering intensity distribution (%) and cumulative absolute frequency (%) of ALs, measured using dynamic light scattering. There are two peaks indicating diameters of ~200 nm (⇩) and 15 700 nm (⇩). (d) Number distribution (%) and cumulative absolute frequency (%) of AL, measured by dynamic light scattering. Approximately 100% of ALs were ~200 nm in diameter (⇩). ALs with diameters exceeding a few micrometers accounted for <0.01%. The arrows (↓) in (c) and (d) indicate the line of the cumulative absolute frequency (%).

2% osmium tetroxide solution, and was fixed at 4°C for 6 h. Dehydration in an ethanol series (50–100%) at room temperature followed, and the solution was embedded in an EPON812 resin mixture at 60°C for 48 h. Thin sections were obtained using an ultramicrotome (Power Tome XL, RMC, Boekeler Instruments, Tucson, AZ, USA). They were stained with 2% uranyl acetate (Merck) for 15 min, washed with rinse solution and were finally stained with a lead stain solution (Sigma, Tokyo, Japan) for 5 min. Histogram of the absolute frequency distribution was obtained from 10 TEM images. The diameter of each AL was measured with rulers.

Brightness analysis

Two sets of TEM images (ALs, and non-gas-containing liposomes [LSs]) were analyzed to assess the average brightness value of the inside of each kind of liposome. The inner area of each liposome on the images was individually selected and its mean brightness value obtained by the ImageJ software (Rasband, W. S., Image J, U. S. NIH, Bethesda, MD, USA, http://rsb.info.nih.gov/ij/, 1997–2009.). For each image, a brightness value of the background was measured and used for normalization. Overstained areas were left out for both types of measurements. Relative brightness values (measured mean brightness/background brightness) were obtained for 106 LSs and 83 ALs.

Statistical analysis

All measurements were represented as either mean ± SD (standard deviation) or SEM (standard error of the mean). Statistical analysis was performed by using Student's *t*-test. Difference with $P < 0.05$ was considered significant. The statistical analysis was performed using Excel 2000 (Microsoft, USA) with the add-in software Statcel 2 [16].

Results

First, the data obtained for ALs and LBs using dark light microscopy were examined, given that both have similar membrane components (Fig. 1a and b). Figure 1a shows that each AL was captured clearly. ALs with a diameter of up to 30 μm existed. Figure 1c shows the percentage of scattering intensity distribution and cumulative absolute frequency of ALs. Two peaks were observed indicating diameters of ~200 nm and 15 700 nm. Figure 1d shows the

Table 1. Bubble characteristics

Nano/microbubble	Shell	Gas	[a]Size (nm)	[b]Zeta potential (mV)
AL	DSPC/DSPE-PEG2000	Perfluoropropane	199 ± 84.4 ($n = 8$)	-2.1 ± 0.9 ($n = 4$)
LB	DSPC/PEG	Perfluoropropane	1222 ± 442.7 ($n = 9$)	-4.2 ± 1.3 ($n = 5$)
AB (Optison)	Albumin	Perfluoropropane	1689 ± 299.8 ($n = 4$)	-40 ± 6.9 ($n = 4$)

[a]Size was measured using dynamic light scattering. Approximately 100% of ALs were ~200 nm in diameter. ALs with diameters larger than a few micrometers accounted for <0.01% (see Fig. 1). Further, 90% of the LBs were ~1200 nm in diameter (data not shown).
[b]The zeta potential was calculated using the Smoluchowski equation.
Values are represented as mean ± SD.

number distribution (%) and cumulative absolute frequency (%), which have been converted from Fig. 1c. Results show that most ALs have diameters of ~200 nm, while ALs with diameters exceeding a few micrometers accounted for <0.01% (Fig. 1c and d). Figure 1b shows the overall LB view. Although large bubbles were visible, the tiny bubbles that were observed in Fig. 1a were not detected in Fig. 1b. The mean diameters for the ALs, LBs and ABs are summarized in Table 1, with AL diameter being one digit smaller than that of the LBs and ABs.

To confirm that the C_3F_8 gas was actually encapsulated by the AL shell, we measured the echogenicity of liposomes sonicated in the presence of either atmospheric air or C_3F_8 gas. Figure 2a shows characteristics of liposomes under either atmospheric air or C_3F_8 gas. Photos show that liposome suspension sonicated in the presence of C_3F_8 is cloudier than that of air and original liposome suspension (NONE). Next we measured echogenicity of each bubble by the method indicated in Fig. 2c. The US B-mode images show that liposome sonicated in the presence of the C_3F_8 gas have a high echogenicity. This tendency is confirmed by the brightness histogram of the liposome sonicated in the presence of the C_3F_8 gas that displays a shift to the right of the brightness levels compared to that with air. Figure 2b indicates the difference of brightness value between liposome sonicated in the presence of either atmospheric air or C_3F_8 gas. The values were normalized by that of NONE. There is a highly significant difference between them ($P < 0.01$).

The zeta potential is one of the primary parameters indicative of drug delivery efficiency, since it informs about dispersivity, aggregability and mutual interaction inside the colloidal suspension. Zeta potential values are summarized in Table 1. ALs and LBs possessed neutral values since neutral lipid phosphatidylcholine was the primary component of their shells and the PEG distributed on their shell surfaces is a nonelectrolyte, water-soluble polymer. ABs had a strong negative charge, indicating that the AB colloid is the most stable of the three bubble types.

Next, ALs were stained using negative staining, and their structures were examined by TEM (Fig. 3). In general, when a lipid bilayer is negatively stained, the stain solution penetrates the lipid bilayer. Existence of gas within certain areas of ALs will prevent that area from being stained effectively, resulting in a reduction in net electron density in that area. The black arrows in Fig. 3a and b indicate the presence of gas within the ALs. Decreased electron density in the central area was apparent in 69 out of 345 ALs, i.e. 20%. The shape of LBs (Fig. 3c and d) was not always spherical as compared to the shapes of ALs. A significant decrease in electron density was not observed in the interior making it difficult to determine whether gas existed in the LB. Figure 3d shows that some LBs had a bag configuration suggesting that an LB may potentially contain both gas and liquid. The AB shell structure caused strong electron beam scattering around the shell (Fig. 3e). As shown in the magnified figure (Fig. 3f), albumin was observed in filament form (indicated by the black arrow), with the layer being several hundred nanometers thick. The interior gas was assumed to be packed in a stable manner and covered with the thick albumin shell. The internal electron density was relatively low, indicating the existence of gas. Figure 4 shows the histogram of the absolute frequency distribution obtained from 10 TEM micrographs. The maximum value was obtained within the class interval of 91–120 nm. This value was about half that measured with dynamic light scattering (see Table 1). Figure 5 shows the distribution of relative brightness values in original liposomes (LSs) and ALs. The statistical distribution of ALs is slightly shifted to relative brightness values closer to 1 compared to the

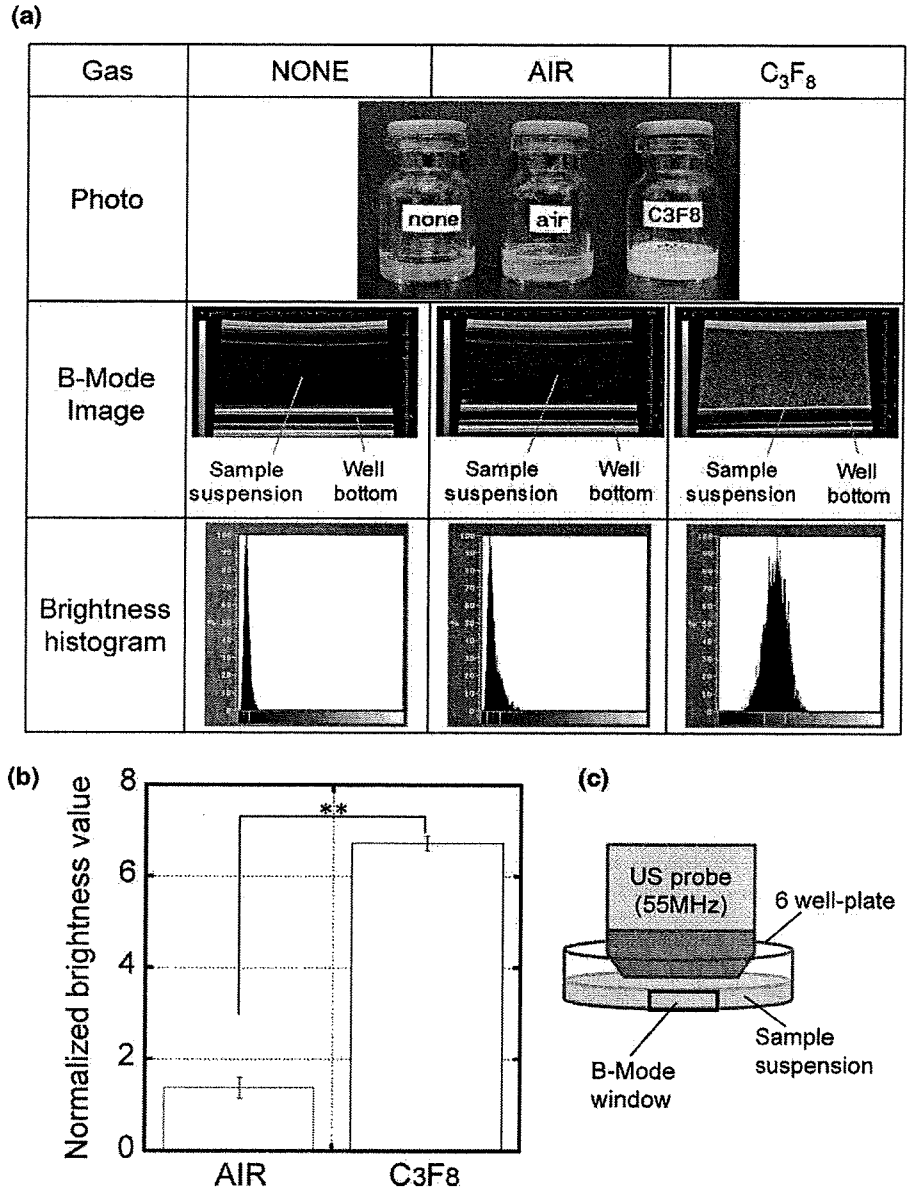

Fig. 2. Confirmation of gas entrapment into liposome. Photos, US B-mode images and brightness histograms of original liposome suspension (none), liposome sonicated under either atmospheric air (air) or C_3F_8 gas (C_3F_8) indicate encapsulation of gas under the presence of the C_3F_8 gas but not in the presence of air (a). The US B-mode images were captured as shown in the scheme for ultrasound imaging (c). There was a highly significant difference in brightness value between liposome sonicated under atmospheric air and C_3F_8 gas. The values were normalized with that of liposome without gas. $n = 4$, mean ± S.E. $^{**}P < 0.01$.

distribution of LSs, indicating that C_3F_8 gas bubbles are actually present inside some of the ALs.

Figure 6 shows a magnified image of the AL, stained at 80°C with the negative staining. The fluidity of lipid layers increases due to heat, and results in the enhanced penetration of the staining solution. The shell thickness was 5.6 nm, which accords with a biomembrane with a thickness of 7–10 nm. Thus, the AL shell is assumed to be a single lipid bilayer.

In order to investigate the AL structure in detail, we observed its cross-section, obtained from the double staining (Fig. 7). The black arrows in Fig. 7a indicate the presence of gas, while the white arrow indicates the presence of liquid. The percentage of